The Dawn of Quantum Biophotonics

Dmitri V. Voronine, Narangerel Altangerel, Edward S. Fry, Olga Kocharovskaya, Alexei V. Sokolov, Vladislav V. Yakovlev, Aleksey Zheltikov, and Marlan O. Scully

D.V. Voronine (✉) • A.V. Sokolov • M.O. Scully
Texas A&M University, College Station, TX 77843, USA

Baylor University, Waco, TX 76798, USA
e-mail: scully@tamu.edu

N. Altangerel • E.S. Fry • O. Kocharovskaya • V.V. Yakovlev
Texas A&M University, College Station, TX 77843, USA

A. Zheltikov
Texas A&M University, College Station, TX 77843, USA

Moscow State University, Moscow, Russia

M.D. Al-Amri et al. (eds.), *Optics in Our Time*, DOI 10.1007/978-3-319-31903-2_7

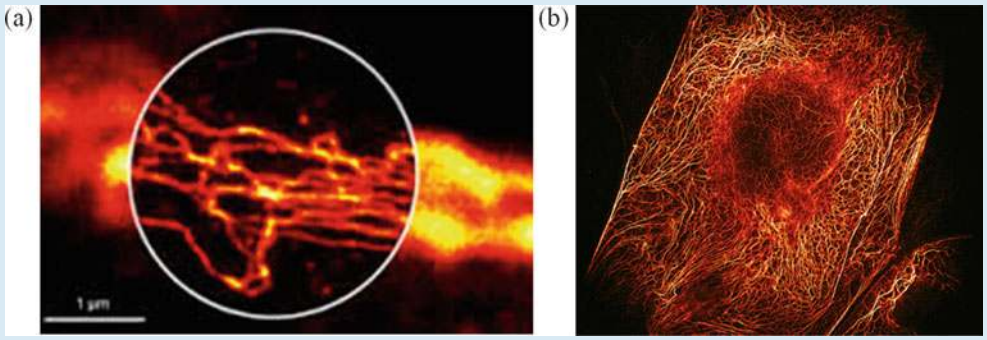

Fig. 7.1 (**a**) STimulated Emission Depletion (STED) microscopy with enhanced resolution (inside the circle) compared with the conventional optical microscopy (outside of the circle). (**b**) REversible Saturable OpticaL Fluorescence Transitions (RESOLFT) image of keratin in cells. Adapted from [1, 2]

7.1 Overview: Toward Quantum Agri-Biophotonics

Quantum mechanics, the crowning achievement of twentieth century physics, is yielding twenty-first century fruit in the life sciences. For example, the broad and multi-faceted field of *Quantum Biophotonics* is exciting and rapidly developing, with many emerging techniques and applications. The broad range of topics includes remote sensing with applications toward plant phenotyping, single cell/virus/biomolecule detection, and superresolution imaging. Progress in the latter was recognized with the 2014 Nobel Prize in Chemistry (Fig. 7.1). New developments in this field are promising and may deliver at least an order of magnitude improvement.

Laser spectroscopy has been widely used for chemical analysis of the living systems. For example, Raman and infrared (IR) spectroscopies can probe the vibrational states of molecules in order to determine, e.g., chemical assay and temperature profile. IR spectroscopy is widely used because it is simple and inexpensive. Raman spectroscopy is more complicated but has many advantages and is a more versatile and powerful tool. Coherent and stimulated Raman techniques can be used to increase the speed and strength of signal acquisition by orders of magnitude. Femtosecond adaptive spectroscopic techniques for coherent anti-Stokes Raman spectroscopy (FAST CARS) was used to detect small amounts of anthrax-type endospores on a nanosecond time scale [3–5] and inside a closed envelope [6]. Fluorescence measurements of fecal matter in water achieved increase of sensitivity by three orders of magnitude [7]. Laser-induced breakdown spectroscopy has been developed to perform studies of plant physiology and phenotyping. Surface-enhanced coherent Raman spectroscopy achieved astonishing results in detection sensitivity [8, 9]. All these techniques are aimed at increasing the speed and reliability of field-based sensing and can be used for improving crop yield. These scientific and technical innovations hold promise for new diagnostic tools bridging the gap between fundamental quantum research and potential agricultural applications.

7.2 Fundamental Light–Matter Interactions and Spectroscopy of Biological Systems

Quantum mechanics provides the most complete description of the light–matter interactions and of the various spectroscopic techniques used for probing the structure–function relations in many fields of science and engineering. These

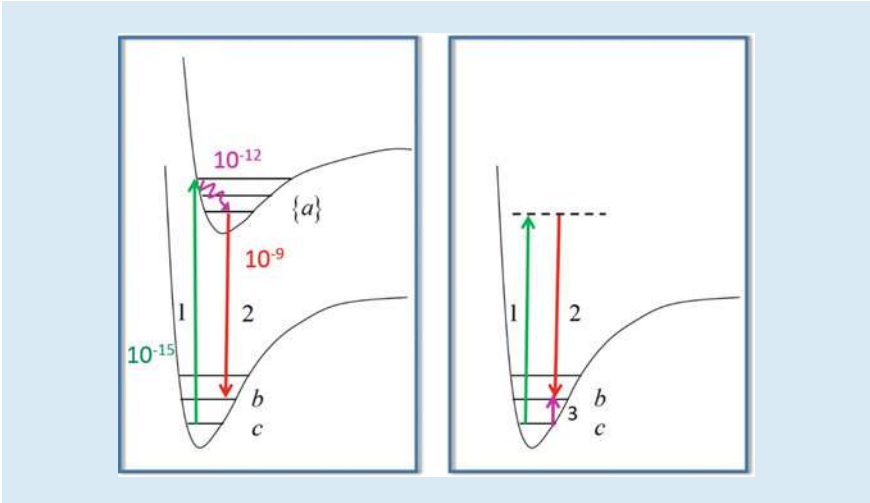

Fig. 7.2 Fundamental light–matter interactions in bio-objects involve absorption, emission, and scattering of light (represented by *arrows*) by molecular systems (represented by *energy level diagrams*). Absorption, relaxation, and fluorescence emission take place on a time scale of 10^{-15} s, 10^{-12} s, and 10^{-9} s, respectively (*left panel*). Non-resonant Raman scattering occurring through a virtual level (*dashed line*) quasi-instantaneously (*right panel*). Infrared absorption (*purple arrow*, *right panel*) provides complimentary information to Raman spectroscopy

interactions happen on different time scales from femtoseconds [~10^{-15} as in the case of absorption shown by a green arrow 1 in Fig. 7.2 (left)] to picoseconds [~10^{-12} as in the case of vibrational cooling shown by a purple wavy arrow in Fig. 7.2 (left)] to nanoseconds [~10^{-9} as in the case of fluorescence emission shown by a red arrow 2 in Fig. 7.2 (left)] and longer. Some processes are almost instantaneous, for example, Raman scattering [shown by red arrow 2 in Fig. 7.2 (right)]. Modern pulsed laser sources with pulse durations from nanoseconds to femtoseconds and beyond can be used to investigate and control these processes. Fluorescence and Raman scattering are major laser spectroscopic techniques which can be used for analytical purposes in agricultural, biomedical, environmental, and many other applications. Infrared absorption also provides complimentary information. Below we describe several examples of recent breakthroughs using these and other techniques within the general field of quantum biophotonics.

The Raman spectroscopic technique is a valuable tool which has excellent potential for the analysis of plant and animal agriculture. Raman spectroscopy is a vibrational measurement which can be applied directly to plant and animal tissues yielding characteristic key bands of individual constituent components. The physics of the Raman effect is analogous to scattering off of an oscillating mirror. It relies on inelastic scattering of light from a laser in the visible, near-infrared, or near ultraviolet range off of molecules. The laser light interacts with molecular vibrations resulting in the energy of the laser photons being down shifted (Stokes) or up shifted (anti-Stokes) signals, respectively (Fig. 7.3). The shift in energy gives useful information about the vibrational modes in the system providing molecular "fingerprints" which can be used for identification. Moreover, essentially all molecules have Raman active vibrational transitions.

Unlike optical absorption transitions, it is possible in principle to separate out the Raman emission of a particular target molecule from the many background molecules in the focal volume. This is because the molecular vibrational levels scatter light with distinctive frequency shifts that are often narrowband. Since there are usually many vibrational transitions in a biomolecule, there are many Raman lines to choose from and these can be used to fingerprint the target molecule. Another important advantage of Raman techniques is that the laser

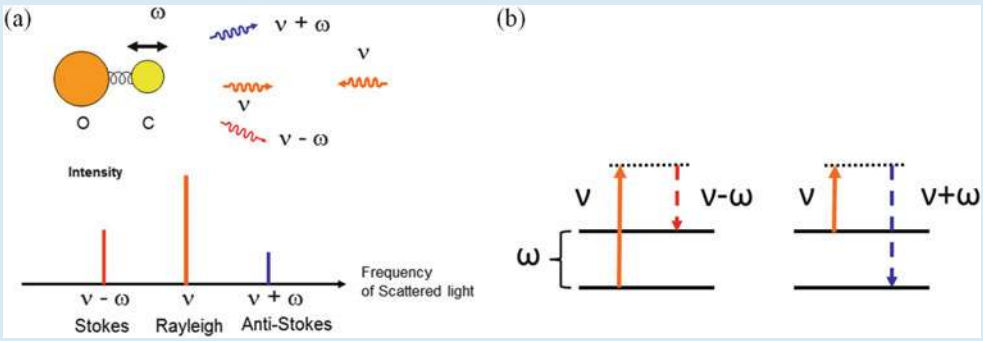

Fig. 7.3 The Raman effect (**a**) and the energy level Stokes and anti-Stokes diagrams (**b**) for a simple molecule. Light at the probe frequency *v* is inelastically scattered off of the molecule resulting in the characteristic frequency shift which serves as a fingerprint for chemical analysis

does not need to be tuned near the optical transition. Even if the optical transition is in the UV, Raman transitions can be efficiently excited with lasers tuned as far away as the near IR, for example, 1064 nm or longer. For such large detunings, the excited state is essentially unpopulated, and so laser damage effects (such as bleaching) or background from chlorophyll fluorescence is strongly suppressed. These features make the Raman approach particularly useful for plant and animal studies which deal with highly complex samples and their environment. Figure 7.4 shows an example of application of Raman spectroscopy for the early detection of anthocyanin markers of stress in plants [10].

Brillouin scattering is another light–matter interaction phenomenon which has delivered an emerging biomedical tool that has already been used to study bone, collagen fibers, cornea, and crystalline lens tissue. Unlike Raman spectroscopy, which offers information about the chemical makeup of the sample, Brillouin spectroscopy provides information about the viscoelastic properties of a material, and consequently, can characterize larger bulk changes. Each of these imaging tools offers useful diagnostic information. Therefore a single apparatus that could provide simultaneous measurement of both spectra from the same point would be extremely powerful for sample characterization and analysis [11]. However, if separate instruments are used, the acquisition time for each Brillouin spectrum is very long (~15 min), making such approach impractical. The lack of the same-point detection for both spectra makes the analysis complicated. To overcome these issues, we recently used a single pump laser to generate both Raman and Brillouin spectra [12] and to provide simultaneous imaging from the selected confocal volume. More importantly, we take advantage of the recent advancements in Brillouin spectroscopy to decrease the acquisition time, as any practical implementation of the simultaneous detection requires that the times for both to be comparable. Unlike other approaches that use scanning Fabry Perot cavities, we utilized a virtually imaged phase array (VIPA), which offers a higher throughput efficiency, >80 %, and does not require scanning to extract a complete spectrum. Subsequently, a VIPA-based system drastically cuts down the acquisition time, which was traditionally a limiting factor in Brillouin spectroscopy. The major challenge in Brillouin spectroscopy of biological systems is eliminating the large amount of elastic scattering, which makes it difficult to identify a weak Brillouin peak. We recently reported that this limitation can be overcome by using a molecular/atomic gas cell as a notch filter [13]. Utilizing these advancements, we demonstrate simultaneous Raman–Brillouin microscopy, a potent new tool for bioimaging and analytical characterization.

Both Raman and Brillouin phenomena arise from the inelastic scattering of light, where the scattering causes the frequency of light to shift in accordance with

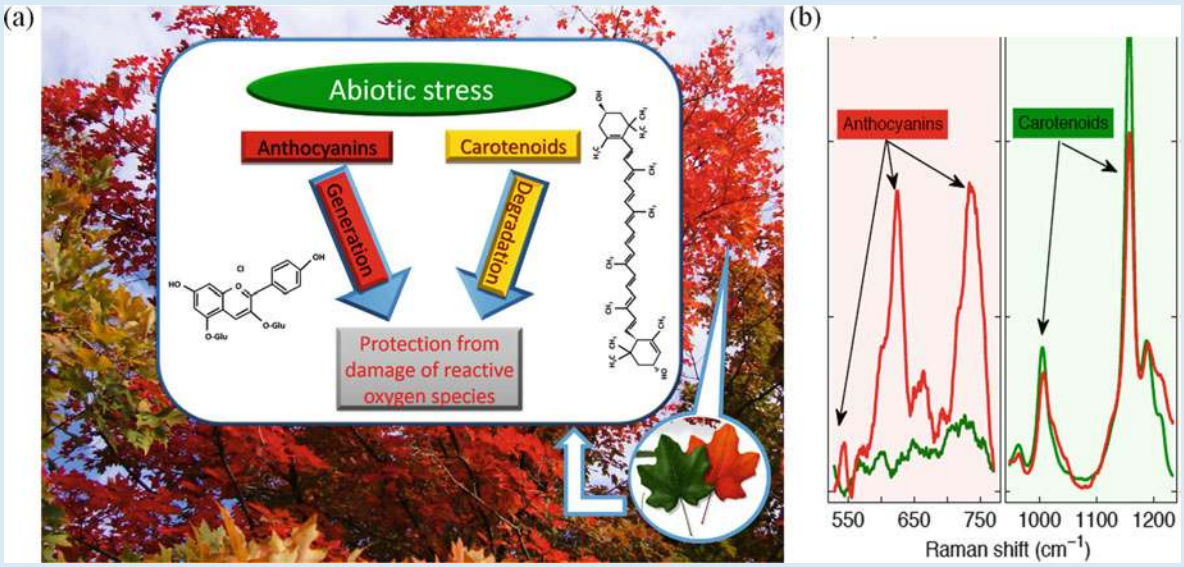

Fig. 7.4 (**a**) The autumn colors of maple trees are due to anthocyanins and are indicative of plant stress. To enhance the survival probability of stressed crops, it is important to identify stressed plants as early as possible to allow for effective intervention. Raman spectroscopy can reveal early spectroscopic signatures of carotenoids and anthocyanins. (**b**) Raman spectra of the unstressed (*green*) and saline stressed (*red*) plants after 48 h. Adapted from [10]

some resonant property. In the case of Raman, the incident light interacts with molecular vibrations causing the light to shift. Similarly, Brillouin scattering is caused by the inelastic interaction of light with periodic fluctuations in a material's index of refraction. From the quantum physics perspective, Brillouin scattering is an interaction between an electromagnetic wave and a density wave (photon–phonon scattering). Thermal motions of atoms in a material create acoustic vibrations, which lead to density variations and scattering of the incident light. These fluctuations carry information about a material's bulk compressibility and viscoelasticity. Whereas Raman scattering can have frequency shifts on the order of 100 THz, Brillouin shifts are only on the order of 10 GHz due to the relatively low energy of the acoustic phonons. The magnitude of the Brillouin shift is dependent upon the collection geometry. Through the measured Brillouin shift we are able to extract mechanical properties of the material, including the speed of sound, adiabatic compressibility, and the longitudinal modulus. While Brillouin scattering is most often used to measure elastic properties of materials, the linewidth of the Brillouin signal also provides information about the viscoelasticity.

The imaging capability of the Raman–Brillouin microscope is shown using a T-shaped sample made of two materials with different mechanical and chemical properties (Fig. 7.5). Cyclohexane and poly(ethylene glycol) diacrylate (PEGDA) hydrogel are model systems, and the hydrogel was cured in a "T"-shaped mold to provide spatial contrast. The body of the T-shaped structure was created using PEGDA. The T-shaped structure was then placed into a solution of cyclohexane, which provided contrast for the image. The corresponding Raman and Brillouin images are shown in Fig. 7.5. In all cases a high-contrast image was produced, whose spatial accuracy can be confirmed when compared to an optical photograph of the sample.

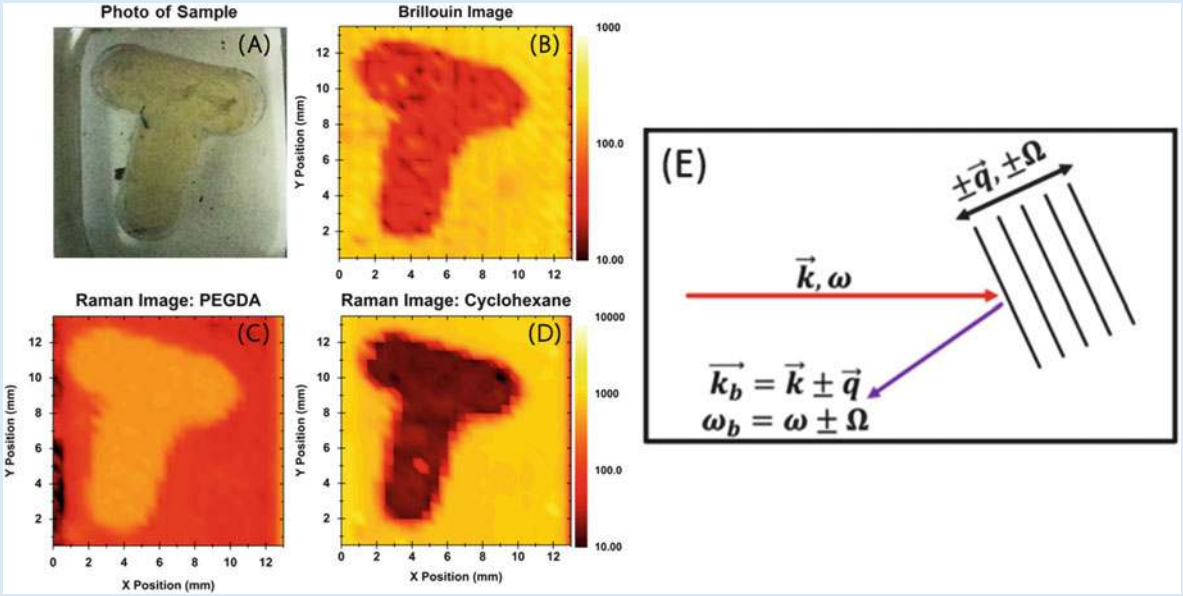

Fig. 7.5 Images of the T-shaped sample: (**a**) Optical photograph; (**b**) Brillouin image using the intensity of the cyclohexane peak at 4.58 GHz as contrast; (**c**) Raman image using the normalized ratio between the PEGDA peaks at ~1400 and ~2800 cm^{-1}; (**d**) Raman image using the cyclohexane peak near 800 cm^{-1} as contrast. (**e**) Schematic diagram of the Brillouin scattering process where incident light interacts with the acoustic field of the material. The magnitude of the frequency shift is dependent upon the direction of light scattered by the acoustic wave. Adapted from [12]

7.3 Quantum-Enhanced Remote Sensing

7.3.1 Anthrax Detection in Real Time

Chemically specific optical imaging and sensing techniques play a pivotal role in developing preventive measures to maintain chemical and biological safety. Frequently, objects to be imaged and identified are not present on a surface, and the light probe has to pass through layers of scattering material. For example, the anthrax-causing bacteria *Bacillus anthracis* can form micron-sized spores which can be present in air, or on the skin of cattle. Brucellosis-causing bacteria *Brucella* spp. can be present in strongly scattering liquids such as milk or blood.

In particular, the detection of anthrax in the farmland environment is an important problem of current interest. Clearly, it would be highly desirable to identify the chemical content of, for instance, air near farm animals, or in wool, and so forth, i.e., identify anthrax spores on-the-fly in air, or image samples of hair in order to chemically distinguish common biological and chemical threats. However, the detection of a chemically specific target in a harsh environment presents several problems. First, targeted molecules are not directly accessible for interrogation, and a remote sensing technique has to be used. On passing through the scattering medium (e.g., wool), both the incident and signal light are substantially diminished, weakening the signal and diffusing the spatial information about the signal's origin. Second, the chemical specificity of anthrax detection has to be maintained in the presence of a substantial background from surrounding chemicals.

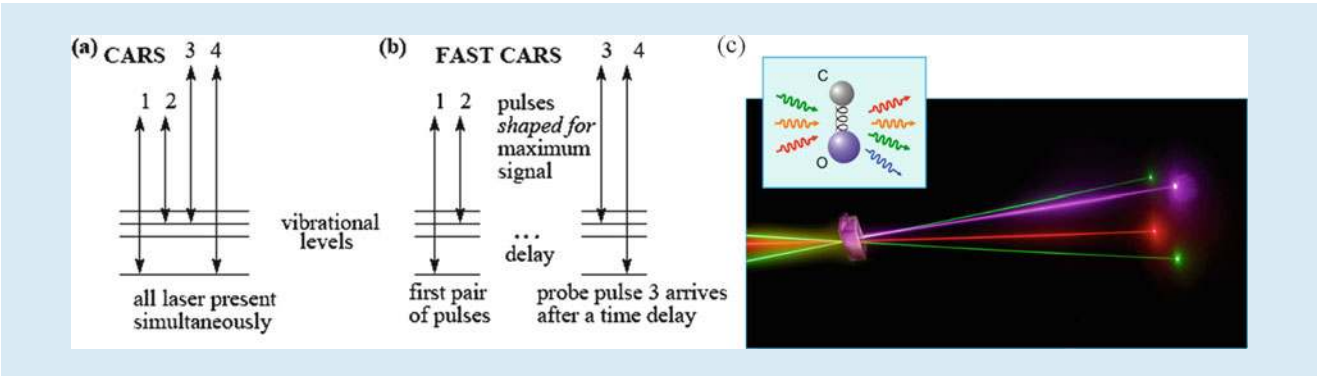

Fig. 7.6 Femtosecond adaptive spectroscopic techniques for coherent anti-Stokes Raman spectroscopy (FAST CARS). Comparison between the energy level schemes and laser configurations for the conventional CARS (**a**) and FAST CARS (**b**). (**c**) Sketch of the laser beam configurations. Inset shows a vibrating molecule emitting signals

7

The major drawback of the commonly used spontaneous Raman spectroscopy is the weak signal strength. We have developed a new spectroscopic technique (FAST CARS) based on maximizing quantum coherence by breaking the adiabaticity** and laser pulse shaping to optimize it. In FAST CARS spectroscopy the signal is proportional to the number of molecules squared, as opposed to the linear dependence in the spontaneous Raman technique [14]. In addition, FAST CARS was the first proposal for background suppression in precision sensing of minor molecular species within a highly scattering environment [3], and provided an efficient solution to the problem of detecting and identifying anthrax-type bacterial endospores in real time [4, 5].

Figure 7.6 shows the basic idea behind the FAST CARS approach. With standard CARS (Fig. 7.6a) two lasers with frequencies ω_1 and ω_2 (we often refer to these lasers as 1 and 2) are incident on a sample. The difference frequency may be resonant with some molecular vibrational excitation. At the same time, the sample may also absorb a third photon (either a third laser with frequency ω_3, or a second photon from laser 1, $\omega_1 = \omega_3$) and generate light at frequency $\omega_4 = \omega_1 - \omega_2 + \omega_3$. Variations of this scheme are numerous. For example, one of the two lasers 1 or 2 might be resonant with an electronic excitation in the molecule.

The problem with these schemes is that the process is masked by four-wave mixing (FWM) in a non-resonant medium. This produces broadband nonlinear generation that can be much larger than the small, vibrationally resonant CARS process. That is, the FWM generation at the detected wavelength range can be much larger than the signal we want to detect that is resonant with a specific molecular vibration. Various techniques have been proposed for suppressing this non-resonant process, including heterodyne detection of the CARS signal and the use of polarization tricks to suppress the undesired signals. FAST-CARS was developed for suppressing the nonresonant background based on pulse shaping and is shown in Fig. 7.6b. Here, all lasers provide short pulses. Pulses 1 and 2 are applied to the sample first and laser pulse 3 is delayed. When laser number 3 is applied to the sample and lasers 1 and 2 are not, non-resonant processes cannot occur. However, beams 1 and 2 will have excited coherence between the vibrational levels in the molecule for which they are Raman resonant. If this coherence last longer than the delay, laser 3 will scatter from the coherence and still produce a

**Two-photon resonant pulses produce $\rho_{bc} \neq 0$ quantum coherence by breaking adiabaticity of the molecular excitation; but off-resonant pulses return the molecule to the ground state as $\rho_{bc} = 0$

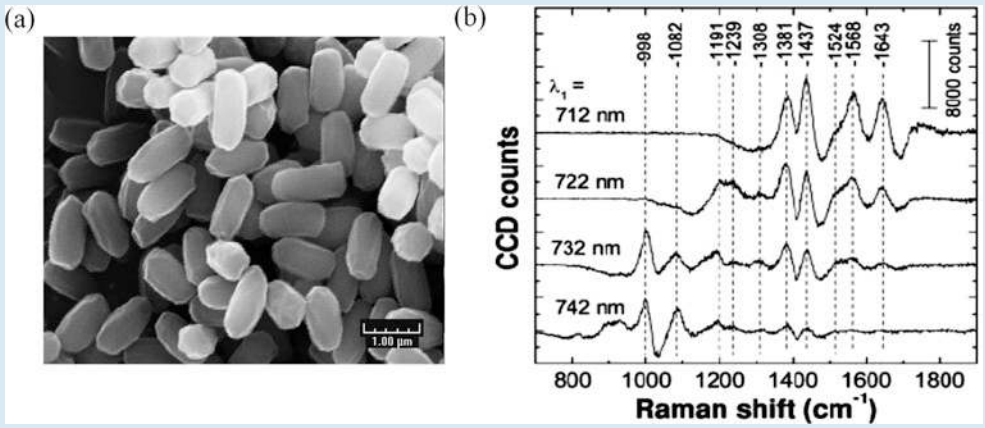

Fig. 7.7 FAST CARS on *Bacillus subtilis* spores (**a**) at various pump wavelengths (λ_1) from 712 to 742 nm (**b**). Adapted from [4]

CARS signal at ω_4. The amount of CARS generation as a function of delay time will show a temporal modulation characteristic of the vibrational energy level structure.

FAST CARS detection of micrometer size *Bacillus subtilis* spores has been performed (Fig. 7.7). A combination of ultrafast pump-Stokes Raman excitation and narrow-band probing of the molecular vibrations provides a species-specific signal from spores [4, 5]. In this scheme, the use of spectrally broad preparation pulses leads to the excitation of multiple Raman lines. The narrow-band probing, on the other hand, allows for frequency-resolved acquisition, as in traditional spontaneous Raman measurements. Recording of the whole CARS spectrum at once makes the technique relatively insensitive to fluctuations. The spectral contrast between the broadband preparation and narrow-band probing provides a way to differentiate between the Raman-resonant and non-resonant contributions. It also helps to mitigate the strength of the non-resonant FWM.

Frequently, objects to be imaged and identified are not present on a surface, and the light probe has to pass through layers of scattering material. In particular, the detection of weaponized anthrax in the mail room is an important problem of current interest. It would be highly desirable to identify the chemical content of an unopened envelope (i.e., image through layers of paper and chemically distinguish common biological and chemical threats from nonhazardous materials). However, the detection of a chemically specific target in a scattering medium presents several problems. First, targeted molecules are not directly accessible for interrogation, and a remote sensing technique has to be used. On passing through the scattering medium, both the incident and signal light are substantially diminished, weakening the signal and diffusing the spatial information about the signal's origin. Second, the chemical specificity of anthrax detection has to be maintained in the presence of a substantial background from surrounding chemicals, such as paper. Recently we demonstrated detection of anthrax-like spores inside a closed envelope using coherent Raman microscopy (Fig. 7.8) [6].

7.3.2 Stand-Off Spectroscopy

The need for an improved approach and efficient tools for remote optical sensing is high since they would facilitate applications ranging from environmental diagnostics and probing to chemical surveillance and biohazard detection. Present-day techniques rely on collecting incoherently scattered laser light and are often hindered by small signal collection efficiency. Availability of a laser-like

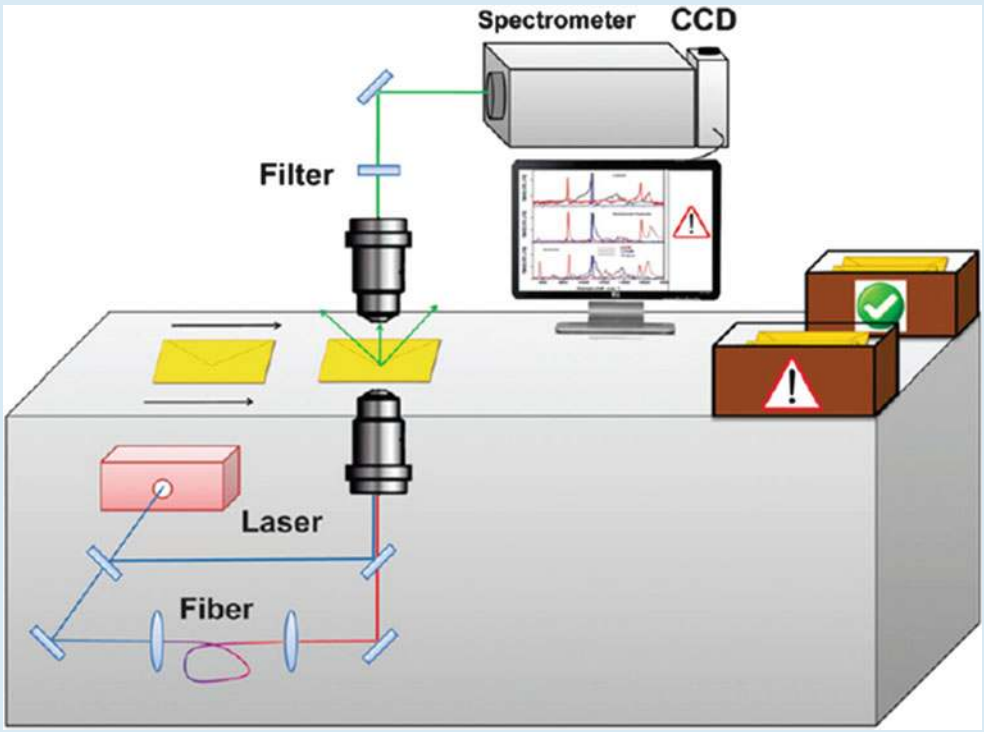

Fig. 7.8 Schematic diagram of the experimental setup for coherent Raman microspectroscopy imaging of anthrax-like spores inside a closed envelope. Adapted from [6]

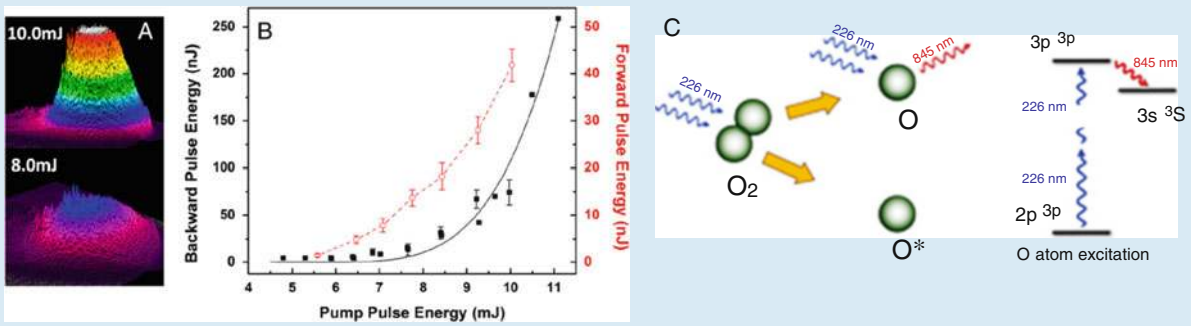

Fig. 7.9 (**a**) Spatial beam profiles of the 845 nm emitted backward pulse at pump energies above (10.0 mJ) and at (8.0 mJ) threshold. (**b**) The energy per pulse of both the forward (*red circles*) and backward (*black squares*) signals versus the pump power. (**c**) Two-photon dissociation of the oxygen molecule and subsequent two-photon resonant excitation of the ground-state oxygen atom fragment result in emission at 845 nm. Adapted from [16, 17]

light source emitting radiation in a controlled directional fashion [15], from a point in the sky back toward a detector, would revolutionize the area of remote sensing. As one example, we have demonstrated the possibility of remote lasing of atmospheric oxygen by using picosecond and nanosecond UV laser pulses that produce atomic oxygen via 226 nm UV pump light, and achieved a bright near-infrared (NIR) laser source at 845 nm wavelength (Fig. 7.9) [16, 17]. Nearly two decades after the work on stimulated emission (SE) performed in the context of flame and flow diagnostics, a renewed interest in laser-like emission from open air is motivated by the need for chemically selective stand-off detection of trace gases in the atmosphere [15].

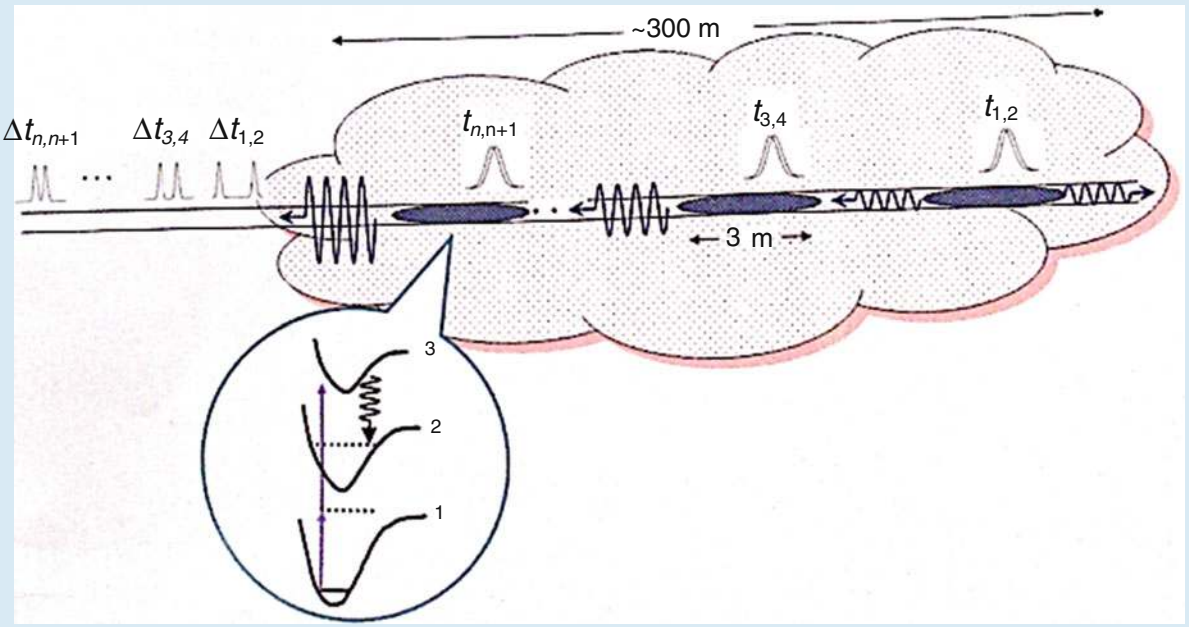

Fig. 7.10 SOS I. Pairs of laser pulses of different colors (e.g., *red* and *blue*) excite a dilute ensemble of molecules in a cloud such that lasing and/or gain-swept superradiance is realized in a direction back toward the observer [18]

Laser-like emission provides a promising tool for a broad class of all-optical stand-off detection methods, as it suggests a physical mechanism whereby a high-brightness, highly directional back-propagating light beam can be generated directly in ambient air. Superradiance can be used to enhance backward-directed lasing in air, using the most dominant constituents such as nitrogen or oxygen. We performed investigations of both the forward and backward-directed emission of oxygen when pumped by nanosecond UV laser pulses. The backward 845 nm beam profile is shown in Fig. 7.9a using nanosecond pulses approximately 10 mJ/pulse of 226 nm. High-quality, strong coherence-brightened emission was observed (Fig. 7.9b).

Earlier, we proposed to use stand-off spectroscopy (SOS) techniques for detecting harmful impurities in air using gain-swept superradiance [18]. In our first SOS scheme it was demonstrated that by using pairs of laser pulses of different colors (e.g., red and blue) it is possible to excite a dilute ensemble of molecules such that lasing and/or gain-swept superradiance is realized in a direction back toward the out-going laser pulses (Fig. 7.10). This approach is a conceptual step toward spectroscopic probing at a distance, also known as SOS [18].

Another simpler approach was developed on the basis of the backward-directed lasing in optically excited plain air (Fig. 7.11). This technique relies on the remote generation of a weakly ionized plasma channel through filamentation of ultraintense trains of femtosecond laser pulses. Subsequent application of an energetic nanosecond pulse or series of pulses boosts the plasma density in the seed channel via avalanche ionization. Depending on the spectral and temporal content of the driving pulses, a transient population inversion is established in either nitrogen- or oxygen-ionized molecules, thus enabling a transient gain for an optical field propagating back toward the source and observer. This technique results in the generation of a strong, coherent, counter-propagating optical probe pulse. Such a probe, combined with a wavelength-tunable laser signal propagating in the forward direction, provides a tool for various remote sensing

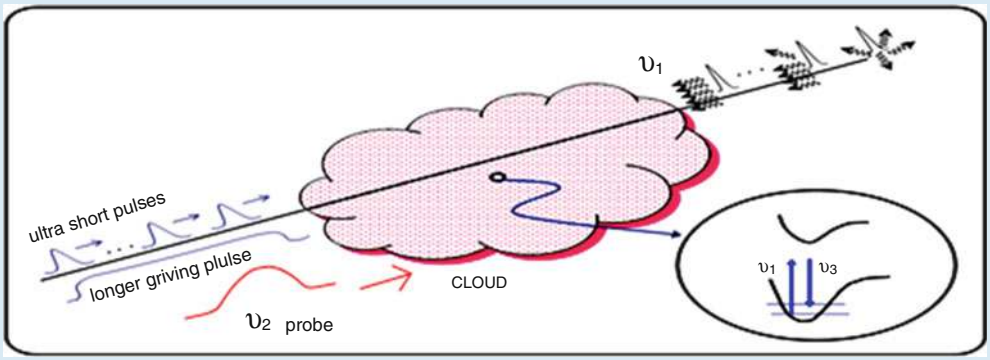

Fig. 7.11 SOS II. An ultrashort laser pulse or sequence of pulses is pre-chirped in such a way that they become compressed by the air dispersion at a pre-arranged distance behind the "cloud." Self-focusing collapse of these pulses results in the generation of weekly ionized "seed" plasma channels. The plasma density in these seed filaments is increased by several orders of magnitude by the application of a longer drive pulse. The properties of the pulses are tailored to produce population inversion in the ionized N_2 and O_2. The air laser radiation at frequency v_1 is combined with an interrogation pulse at v_2 to identify trace amounts of gas in the cloud. Adapted from [15]

7

applications. The technique could be implemented to probe the air directly above the growing crops and has the ability to pinpoint local areas of infection.

7.3.3 Detection of Plant Stress Using Laser-Induced Breakdown Spectroscopy

Remote sensing applied to detection of stress in plants is a very promising field. Plant stress affects the yield of agriculturally and economically significant plants. Rapid detection of plant stress in the field may allow farmers and crop growers to counter the effects of plant stress and increase their crop return. Plants can be affected by many types of stress including drought, pollution, insects, and microbial infestations which have a negative impact on agriculturally and economically significant florae. Rapid detection with little sample preparation is necessary to scale the sensing technology to the field size. We have recently applied laser-induced breakdown spectroscopy (LIBS) to plant stress detection. LIBS provides the advantages of rapid remote sensing [19]. LIBS measurements are performed on plants by focusing a laser pulse onto the surface of a sample causing ablation and vaporization of the sample material forming a plasma plume. The hot plasma with initial temperatures of up to 100,000 K expands and cools, emitting photons of characteristic frequencies from thermalized atomic constituents. LIBS can also be applied to detect other types of plant stress and other elements for phenotyping. For instance, cotton, a staple crop of Texas, is subject to various pestilences such as Southwestern rust (*Puccinia cacabata*), Alternaria leaf spot (*Alternaria macrospora*), and various types of boll rots. LIBS experiments can be performed using lab-based and portable femtosecond laser systems. We performed LIBS measurements for rapid analysis of the effects of drought stress on gardenia and wheat using a lab-based amplified femtosecond laser system operating at ~800 nm center wavelength, with a pulse duration of ~35 fs. We observed significant differences in the LIBS signals from stressed (not watered) and non-stressed (watered) plants and identified several atomic emission peaks as spectroscopic signatures of plant stress which agreed closely with macro- and micronutrients acquired by plants from the soil and air (Fig. 7.12). The LIBS technology may be able to identify key abiotic stress signals and improve the prediction of abiotic stress response capacity and can be used as a rapid remote sensing platform in the field.

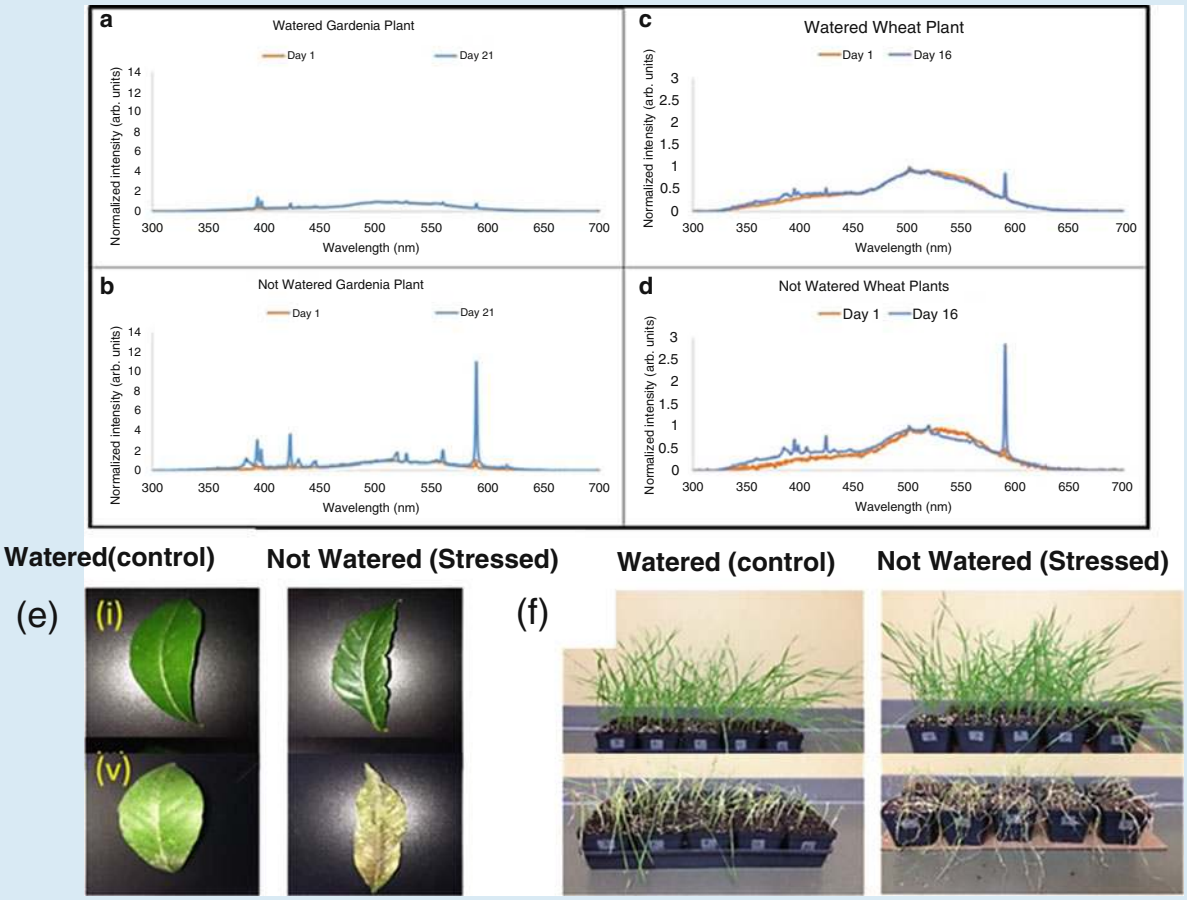

Fig. 7.12 (**a**–**d**) Averaged LIBS spectra of watered (non-stressed) and not watered (stressed) gardenia and wheat plants. The corresponding photographs of the gardenia leaves (**e**) and wheat plants (**f**) taken on the first and last day of the treatment

7.3.4 Stand-off Detection Using Laser Filaments

Femtosecond filamentation has been observed for various pulse durations (from several tens of femtoseconds to picoseconds) and wavelengths (from UV to IR). Due to the presence of high intensity electromagnetic field $I(r, t)$ the refractive index of the medium has the form $n = n_0 + n_2 I(r, t)$, where the nonlinear Kerr index n_2 leads to an interesting effect of the curvature of wave front acting like a focusing lens ($n_2 > 0$) since the intensity is usually the highest at the center of the beam. The latter leads to self-focusing which can overcome the diffraction and leads to the collapse if the input peak power P_{in} exceeds a critical threshold value P_{cr}. Filaments may be also used to induce rain via water condensation in the atmosphere and to induce lightning via electron condensation.

Filamentation of ultrashort laser pulses in the atmosphere offers unique opportunities for long-range transmission of high-power laser radiation and stand-off detection. With the critical power of self-focusing scaling as the laser wavelength squared, the quest for longer-wavelength drivers, which would radically increase the peak power and, hence, the laser energy in a single filament, has been ongoing over two decades, during which time the available laser sources limited filamentation experiments in the atmosphere to the near-infrared and

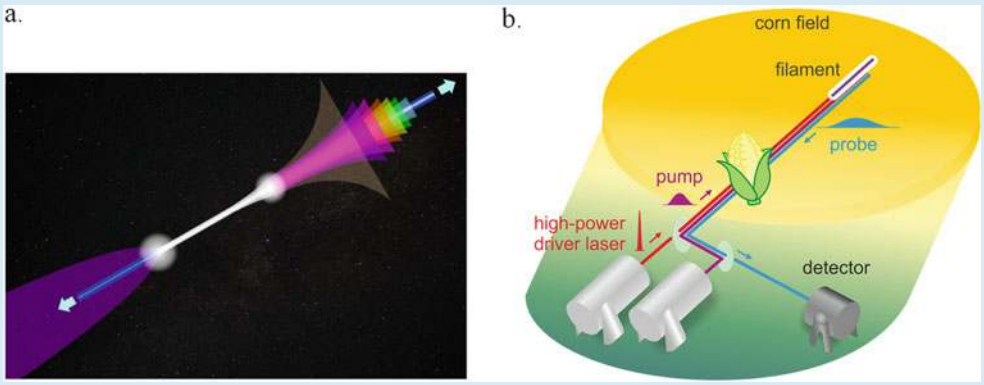

Fig. 7.13 (**a**) Laboratory prototype of a unique mobile high-power laser source of ultrashort pulses in the mid-infrared allows filamentation of ultrashort mid-infrared pulses in the atmosphere. (**b**) This innovative technology offers unprecedented opportunities for long-range signal transmission, delivery of high-power laser beams, and remote sensing in agricultural applications. Adapted from [20]

7

visible ranges. Recently, a unique high-power laser source of ultrashort pulses in the mid-infrared has been created, allowing filamentation of ultrashort mid-infrared pulses in the atmosphere to be demonstrated for the first time with the spectrum of a femtosecond laser driver centered at 3.9 μm, right at the edge of the atmospheric transmission window, radiation energies above 20 mJ and peak powers in excess of 200 GW that can be transmitted through the atmosphere in a single filament (Fig. 7.13) [20]. These studies revealed unique properties of mid-infrared filaments, where the generation of powerful mid-infrared supercontinuum is accompanied by unusual scenarios of optical harmonic generation, giving rise to remarkably broad radiation spectra, stretching from the visible to the mid-infrared. These thrilling discoveries open new horizons in ultrafast optical physics and offer unique opportunities for long-range signal transmission, delivery of high-power laser beams, and remote sensing of the atmosphere [21, 22]. Filament-induced breakdown spectroscopy may be realized as a remote extension of LIBS which was described in the previous section.

7.4 Quantum Heat Engines

Photonic quantum heat engines typically produce useful work by extracting energy from a high temperature thermal photon source, e.g., the Sun, and rejecting entropy to a low temperature entropy sink, e.g., the ambient room temperature surroundings. Lasing without inversion (LWI) is based on induced quantum coherence in the atoms, molecules, and solid state electrons involved. The early careful analyses of LWI were carried out by Kocharovskaya [23] using dark state, i.e., initial coherence; and Harris [24] using Fano interference, i.e., noise-induced coherence. Another related phenomenon is the correlated emission laser [25] which uses radiatively induced coherence to suppress absorption. It has also been shown that quantum coherence can be used to suppress absorption and obtain LWI [26].

More recently, it has become apparent that quantum coherence can be used to break detailed balance in a photocell and thus suppress recombination. This can increase quantum efficiency [27] and enhance thermodynamic power [28]. This reveals the deep connection between lasers and photovoltaic cells. It was shown that it is possible, in principle, to double the power of a thin medium photocell and/or the power of a laser. Finally it was also shown how quantum noise can be

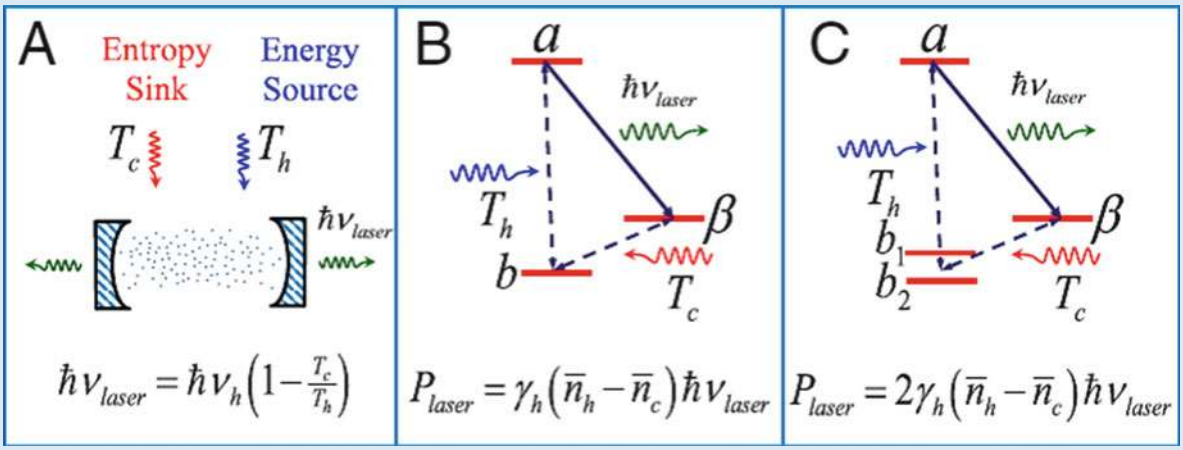

Fig. 7.14 (**a**) Schematic of a laser pumped by hot photons at temperature T_h (energy source, *blue*) and by cold photons at temperature T_c (entropy sink, *red*). The laser emits photons (*green*) such that at threshold the laser photon energy and pump photon energy is related by the Carnot efficiency relation. (**b**) Schematic of atoms inside the cavity. Lower level *b* is coupled to the excited states *a* and β. The laser power is governed by the average number of hot and cold thermal photons, $\bar{n}_h$ and $\bar{n}_c$. (**c**) Same as (**b**) but lower level *b* is replaced by two states b_1 and b_2, which can double the power when there is coherence between the levels. Adapted from [28]

used in the spirit of a quantum heat engine to explain the appearance of coherent oscillations and to increase of efficiency in photosynthesis [29].

7.4.1 The Laser and the Photovoltaic Cell as a Quantum Heat Engine

The arch-type example of a quantum heat engine is a laser pumped by hot thermal light as in Fig. 7.14. Then the frequency of a laser pumped by such narrow band hot light and cooled by narrow band cold light as well as the open circuit voltage of a solar cell or photo-detector obeys the Carnot relations.

However, it is possible to use quantum coherence to go beyond both of these Carnot relations. For example, including quantum coherence in the lower laser state, as in Fig. 7.14, yields the increase in quantum efficiency for the laser. Likewise it is possible to use quantum coherence to increase voltage quantum efficiency for the photovoltaic cell (Fig. 7.15). However one might well wonder if would that not violate the second law of thermodynamics? The answer is no. Quantum mechanics does allow us to get more energy from a thermal reservoir than a classical Carnot engine can, but at a cost. Overall the Carnot limit applies, but in a subsystem we can do better than the Carnot limit. A clean example of this is the photo-Carnot quantum heat engine which we discuss next.

7.4.2 The Photo-Carnot Quantum Heat Engine

The photo-Carnot engine is simply a piston engine in which photons replace the molecules as the driving fluid, as in Fig. 7.16. As such, the photons are like the steam molecules of a steam engine. However, the thermal photons are generated in

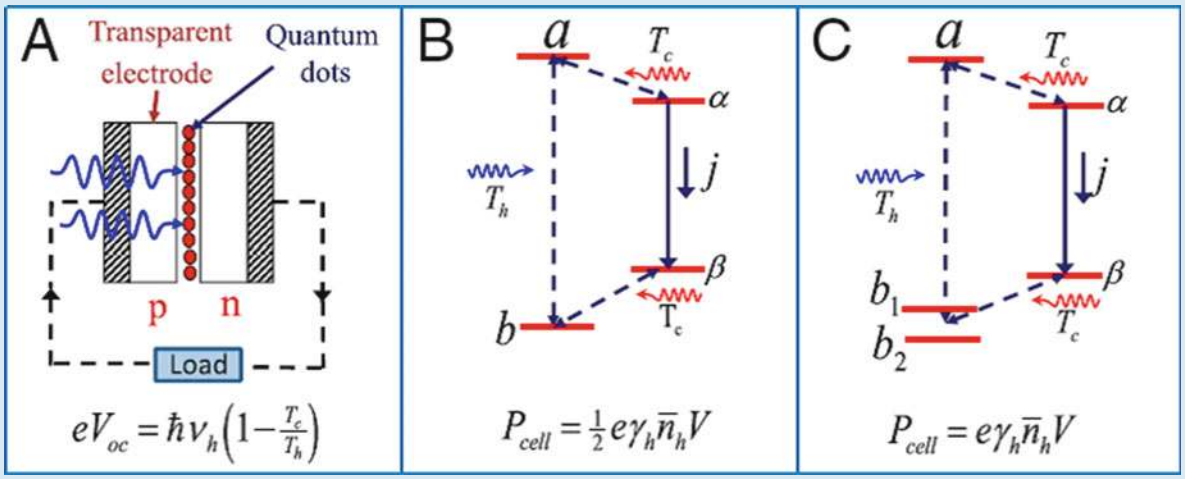

Fig. 7.15 (**a**) Schematic of a photocell consisting of quantum dots sandwiched between *p* and *n* doped semiconductors. Open circuit voltage and solar photon energy $\hbar\nu_h$ are related by the Carnot efficiency factor in which T_c is the ambient and T_h is the solar temperature. (**b**) Schematic of a *quantum dot* solar cell in which state *b* is coupled to *a* via, e.g., solar radiation and coupled to the conduction band reservoir state α via optical phonons. The electrons in state α pass to valence band reservoir state β via an external circuit, which contains the load. (**c**) Same as (**b**) but lower level *b* is replaced by two states b_1 and b_2, and when coherently prepared can double the output power. Adapted from [28]

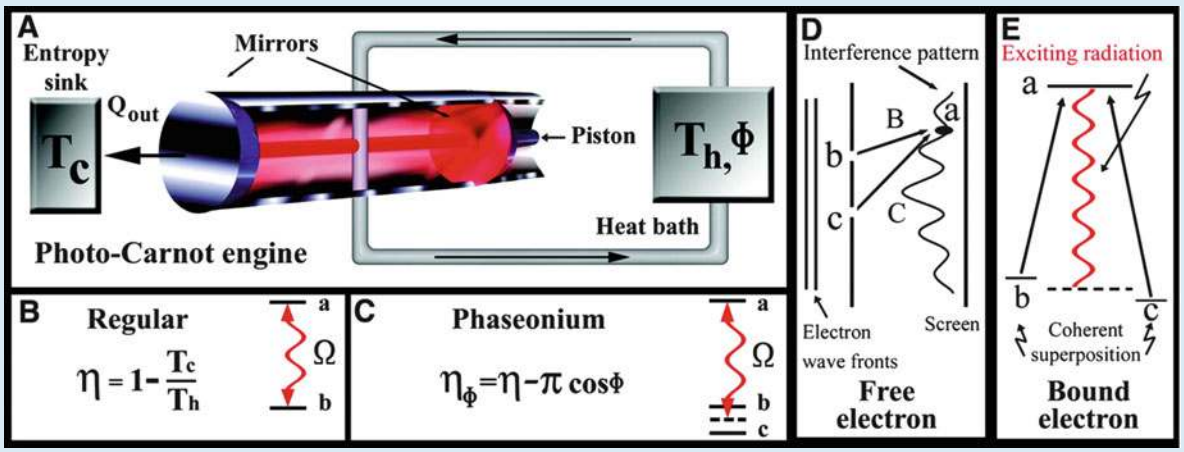

Fig. 7.16 (**a**) Photo-Carnot engine in which radiation pressure from a thermally excited single-mode field drives a piston. Atoms flow through the engine and keep the field at a constant temperature T_{rad} for the isothermal $1 \rightarrow 2$ portion of the Carnot cycle. Upon exiting the engine, the bath atoms are cooler than when they entered and are reheated by interactions with the hohlraum at T_h and "stored" in preparation for the next cycle. The combination of reheating and storing is depicted in (**a**) as the heat reservoir. A cold reservoir at T_c provides the entropy sink. (**b**) Two-level atoms in a regular thermal distribution, determined by temperature T_h, heat the driving radiation to $T_{rad} = T_h$ such that the regular operating efficiency is given by η. (**c**) When the field is heated, however, by a phaseonium in which the ground state doublet has a small amount of coherence and the populations of levels *a*, *b*, and *c* are thermally distributed, the field temperature is $T_{rad} > T_h$, and the operating efficiency is given by $\eta_\phi = \eta - \pi\cos(\phi)$. (**d**) A free electron propagates coherently from holes *b* and *c* with amplitudes *B* and *C* to point *a* on screen. The probability of the electron landing at point *a* shows the characteristic pattern of interference between (partially) coherent waves. (**e**) A bound atomic electron is excited by the radiation field from a coherent superposition of levels *b* and *c* with amplitudes *B* and *C* to level *a*. The probability of exciting the electron to level *a* displays the same kind of interference behavior as in the case of free electrons; i.e., as we change the relative phase between levels *b* and *c*, by, for example, changing the phase of the microwave field which prepares the coherence, the probability of exciting the atom varies sinusoidally. Adapted from [30]

the piston cylinder (electromagnetic cavity) of Fig. 7.16, by the hot atoms; that is, the atoms are the fuel, like the coal in a steam engine. Hence the classical photon driven heat engine must operate (at best) with Carnot thermodynamic efficiency since it is, at bottom, just another heat engine.

However, the plot thickens when we bring quantum coherence into the system. Now the (fuel) atoms can add more heat to the photon flux (working fluid) than was allowed by classical statistical mechanics, i.e., than was allowed by detailed balance. When we use quantum fuel (phaseonium) we can now "beat" the Carnot limit because we can now break detailed balance as per Fig. 7.16 [30]. This is a useful example to bear in mind when thinking about the quantum PV cell and photosynthesis.

7.4.3 Biological Quantum Heat Engines

Quantum entanglement [31] and other quantum coherence effects, e.g., the photon echo [32–36], have been investigated in a series of interesting photosynthesis experiments. The field of quantum biology of photosynthesis has been rapidly growing since the discovery of quantum coherence effects in the energy transfer process of the photosynthetic green sulfur bacteria [32, 35] and marine algae [33]. However, neither the role of quantum coherence nor the precise mechanism of the highly efficient energy transfer has been identified. Their description requires re-evaluation of the currently used methods and approximations. Also, whether the coherence is generated by coherent laser pulses used in the experiments or whether there is a kind of spontaneous coherence between the quantum levels involved as in the sense of noise-induced Fano-Agarwal interference has been the subject of debate. This latter possibility has been observed in various contexts and is indeed well known in quantum optics as described with applications to laser and solar cell quantum heat engines [27, 28, 37]. However it is not clear whether the quantum optical lore has applicability to photosynthesis for several reasons. High on the list being the question of environmental decoherence.

Recently, we have applied the formalism of the quantum heat engines to photosynthetic complexes such as light-harvesting antennae and reaction centers (RC) (Fig. 7.17). These systems operate as quantum heat engines and their structure is suitable to provide an increase in the efficiency of these processes. Connections between various quantum mechanical effects, namely the coherence/population coupling in photosynthesis [29, 38], and the quantum yield enhancement in laser and solar cell quantum heat engines [27, 28] were investigated. Analogy was drawn with a solar cell operation where the electron transfer efficiency may be increased by a quantum coherence between a doublet of closely lying states. It was proposed that the special pair of molecules in RC has a suitable structure to exhibit similar quantum effects. Figure 7.17 depicts the proposed schemes in which the efficiency of the electron transfer from the donor molecule (D) to the acceptor (A) may be increased by the quantum coherence between two donor molecules D_1 and D_2 of the special pair. This can provide insight into the structure–function relations of natural molecular architecture and will inspire new nature-mimicking artificial designs.

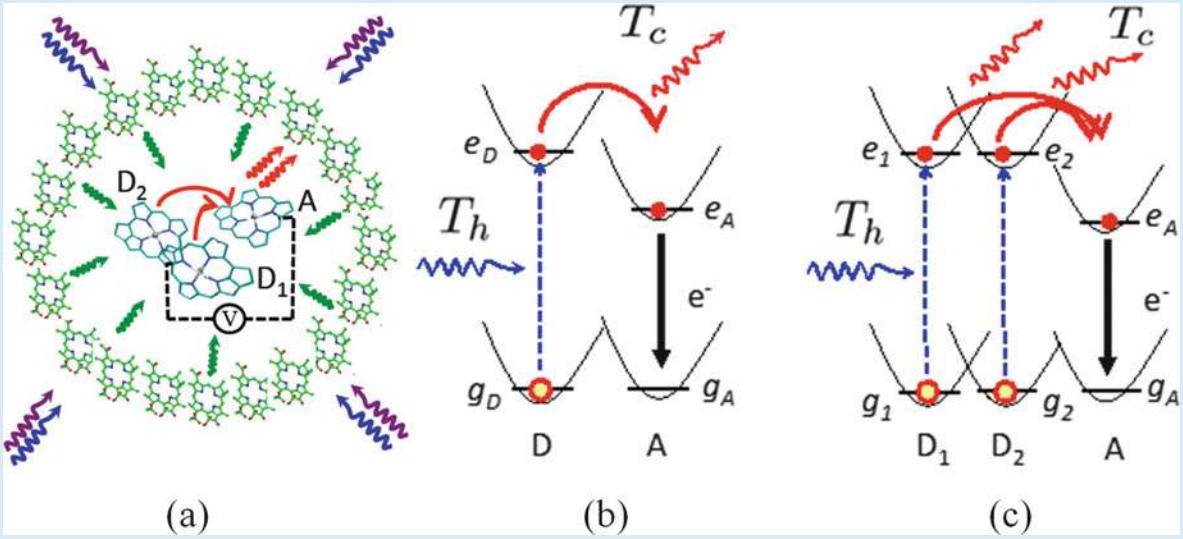

Fig. 7.17 Structure of a reaction center (RC) surrounded by photosynthetic antenna molecules (**a**). Schemes of the charge separation in the toy model of the biological quantum heat engine based on RC (**b**). The narrow band thermal radiation is transferred from the antennae complexes to the RC represented by donor (D) and acceptor (A) molecules. (**c**) Is the same as (**b**) with the upper level a is replaced by two levels a_1 and a_2. Quantum coherence between these levels can increase the power delivered by such a device. Adapted from [29]

7.5 Emerging Techniques with Single Molecule Sensitivity

7.5.1 Coherent Surface-Enhanced Raman Spectroscopy

Biological samples may be analyzed using fluorescence labeling nano-sensing technology such as enzyme-linked immunosorbent assay which is based on antibodies for detection of the presence of specific substances. The principle of this technique is based on the modification of the refractive index of the sensor when the antigen of interest is present. The sensitivity can be further enhanced by placing plasmonic nanoparticles so as to allow surface-enhanced Raman spectroscopy (SERS). These very sensitive techniques can be used to detect extremely small amounts of antigens.

Other techniques such as label-free optofluidic nanoplasmonic sensors have recently shown promise for detection of live viruses in biological media (Fig. 7.18) [39]. Such sensors are based on antibodies immobilized on plasmonic nanostructures such as arrays of small holes in gold or silver chips. These sensors show significantly modified properties of scattered or transmitted light due to the capture of viruses by the attached antibodies. This technology is promising for early diagnosis of pathogens from human blood.

Recently we developed a time-resolved surface-enhanced CARS (tr-SECARS) technique where the gain in signal was attributed to the enhanced electromagnetic fields that are created near the metal particles and in the gaps between the particles or features on the tailored substrates (Fig. 7.19) [8]. Thus the molecules of interest experience these enhanced fields by being attached to or simply near these metal particles or features. This coherent extension of the SERS technique provides an additional signal enhancement due to laser-induced vibrational coherence. It also provides the possibility to study biological systems simultaneously with a high

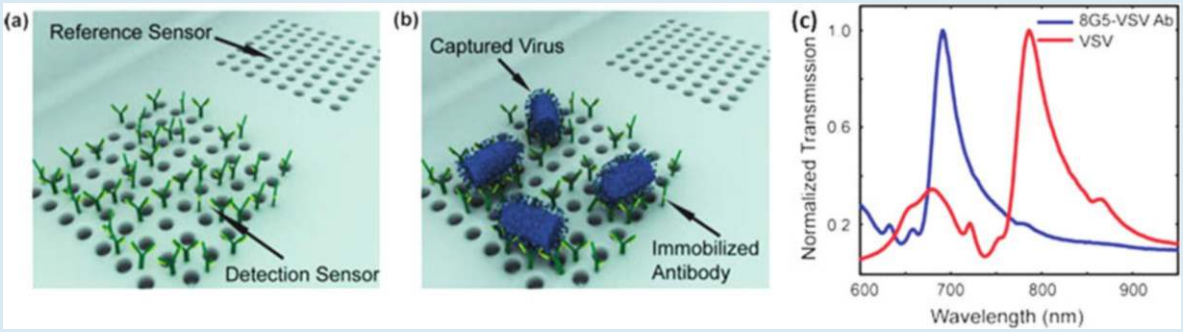

Fig. 7.18 Detection of viruses captured by immobilized antibodies on optofluidic nanoplasmonic sensors (**a**, **b**). Spectra of light transmitted by small holes change due to the capture of viruses (**c**). Adapted from [39]

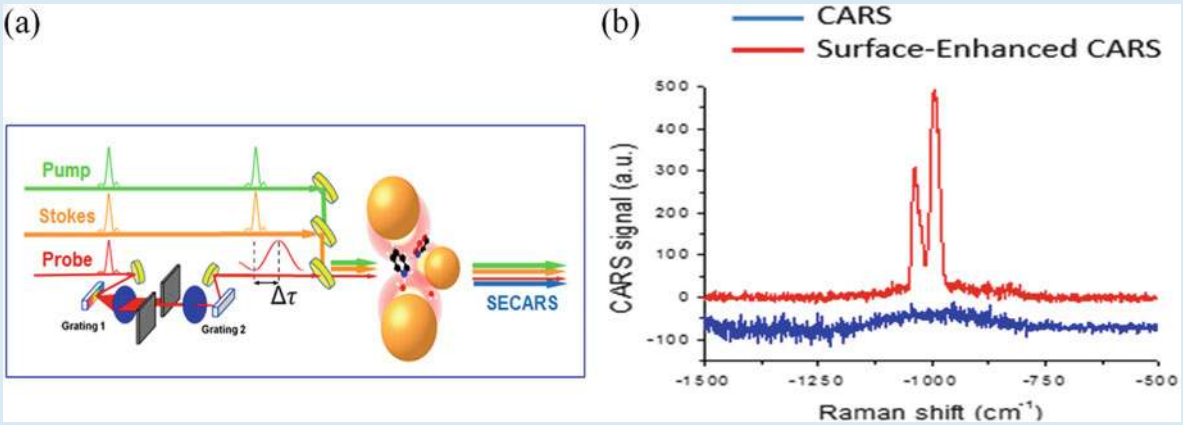

Fig. 7.19 (**a**) Experimental scheme of the time-resolved surface-enhanced anti-Stokes Raman scattering (tr-SECARS) spectroscopy. (**b**) Surface-enhanced CARS (*red*) reveals traces of hydrated pyridine molecules on the surface of gold nanoparticle aggregates with higher sensitivity than the conventional CARS (*blue*). Adapted from [8]

spatial and temporal resolution. Such a SECARS technique has the best-of-both-worlds combination of signal enhancements, i.e., the surface and coherence enhancements. This tr-SECARS technique increased the CARS signal intensity by seven orders of magnitude and was used to detect trace amounts of water on the surface of aggregated gold nanoparticles [8]. Conventional SERS was not able to detect any signal under the same conditions. This was recently reviewed in the literature as having "astonishing" sensitivity [9].

7.5.2 Cavity Ring-Down Spectroscopy

Food and water are essential for life, thus maintaining the safety of these resources is a high priority. The existing problem will only get worse in the years to come, due to limited fresh water supplies and increasing impacts of contaminants on the environment. Importantly, the ability to detect and manage environmental

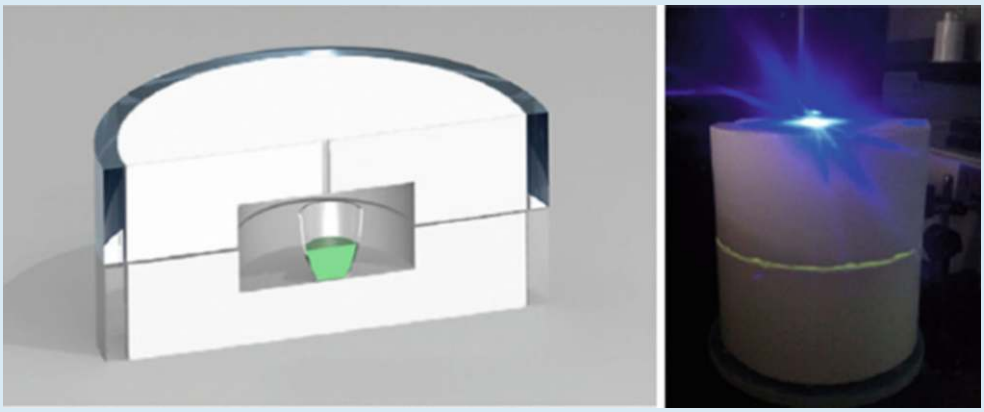

7

Fig. 7.20 Integrating cavity setup for ultrasensitive detection of waste products such as urobilin in water. Adapted from [7]

contamination in food and water (in real time) is a critical need for the assessment and reduction of risk.

Traditional epi-illumination fluorescence spectroscopy systems use an objective lens to focus excitation light into the sample and collect the fluorescence emission. In such a configuration, the generated signal is limited to the focal volume of the optics, and is diffusive in nature; only a small fraction of the total emitted light is collected. Because only a small volume of a sample can be probed at any given time with such a configuration, detection of subnanomolar concentrations remains difficult. Thus, a method that could allow for exciting a larger volume of a sample while also providing means for collecting more of the fluorescence emission could greatly enhance the ability to detect sub-picomolar concentrations of, for example, urobilin (Fig. 7.20).

To achieve both of these goals, an integrating cavity was recently used to enhance both the excitation and collection efficiency [7]. Integrating cavities, especially spherical cavities, are commonly used to measure the total radiant flux from a source, as a means to generate uniform illumination, and as pump cavities for lasers. The high reflectivity of the cavity walls leads to a very large effective optical path length over which fluorescence excitation occurs; and the result is excitation of the entire volume of any sample placed inside the cavity. The high reflectivity of the cavity walls also means that fluorescence is collected from all directions; the result is the ability to detect a 500 femtomolar concentration of urobilin [7].

An accurate knowledge of the spectral absorption of cells and their constituents is critical to the continuation of progress in the understanding and modeling of biological and biomedical processes. Modeling of highly scattering cellular media, imaging of tissues, cells, and organelles, and laser-based surgical procedures are just a few of the vast number of techniques and procedures that rely on a refined understanding of biological absorption coefficients. Previously absorption measurements have generally been performed using transmission-style experiments in which an attenuation coefficient is measured by observing the decrease in the intensity of a light source as it passes through a sample. While the attenuation coefficient includes the losses due to absorption, it also includes the contribution from any scattering present in the sample. But these problems are avoided by using an integrating cavity for absorption measurements. Specifically, due to the nearly Lambertian behavior of the cavity walls, an isotropic field is created inside the cavity and scattering within the sample cannot change that. The result is absorption measurements that are independent of scattering. The integrating cavity technique was used to obtain what are now widely considered

to be the standard reference data for pure water absorption [40, 41]. Cavity ring-down spectroscopy (CRDS) is a technique developed for highly accurate and sensitive measurements of low absorption coefficients. It involves sending a temporally short laser pulse into a high-finesse two mirror cavity and observing the exponential decay, or "ring-down" of the intensity due to absorption (and scattering) inside the cavity. While CRDS is a very powerful technique, it is inherently unable to distinguish the losses due to absorption from losses due to scattering. Much like other transmission-style experiments, it is the attenuation that is being measured. This is clearly a problem for determining weak absorption in highly scattering samples. The new approach is based on CRDS and is called integrating cavity ring-down spectroscopy (ICRDS) where the traditional two mirror cavity used in CRDS is replaced with an integrating cavity. Again, the integrating cavity walls are fabricated from a highly diffuse reflecting material which creates an isotropic light field inside the cavity; the result is that a measurement of the decay time for the optical pulse is inherently insensitive to any scattering in the sample. Thus, ICRDS can provide a direct measurement of the absorption coefficient, even in the presence of strong scattering. However, ICRDS has not previously been implemented because a material with a sufficiently high diffuse reflectivity was not available. Spectralon has been the material with the highest known diffuse reflectivity (99.3 %) [42], but at this level of reflectivity, the decay of the optical pulse due to losses during reflection from the wall is so large that the sensitivity to absorption is low.

A new material has now been developed that has a diffuse reflectivity up to 99.92 % [43]; this is sufficient to make ICRDS a reality. It opens up a plethora of exciting new applications with tremendous impact in, for example, the biomedical area where highly accurate absorption spectra of living cells, tissue samples, liquids, etc., can now be obtained, even when the absorption is very weak compared to scattering in the sample.

As a specific such example, consider human retinal pigmented epithelium (RPE) cells. Among other functions, RPE cells are responsible for absorbing scattered light to improve the optical system and reduce stress on the retina. Figure 7.21 shows an example in which ICRDS was used to measure the base absorption (i.e., with the pigment removed) of 60 million RPE cells in a 3 mL solution [44]. Also shown is the attenuation (scattering plus absorption) spectrum obtained with the same sample in a spectrophotometer. As an example of the dominance of scattering in the transmission measurement, consider the

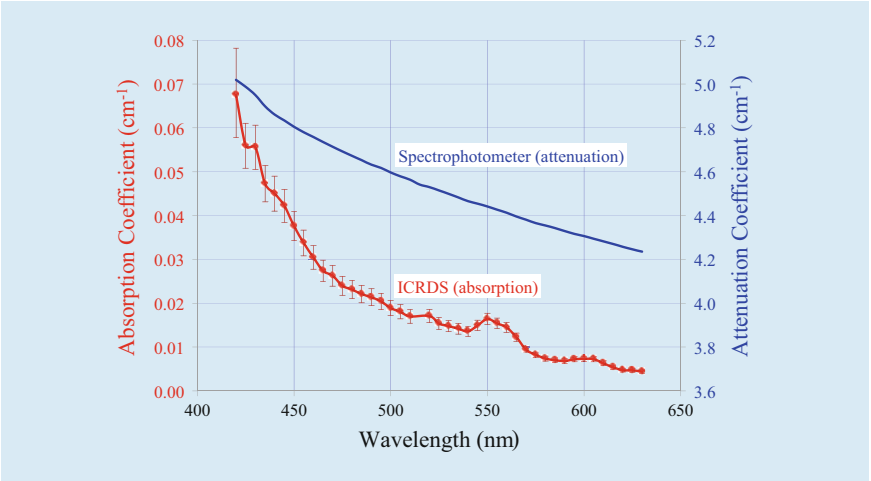

Fig. 7.21 Absorption coefficient of 6×10^7 human retinal pigmented epithelium (RPE) cells in a 3 mL solution; also shown is the attenuation (scattering + absorption) spectrum. Adapted from [44]

attenuation at 500 nm (4.6 cm^{-1}) and the absorption (~0.02 cm^{-1}). This is a factor of 230; the absorption is less than one-half of 1 % of the attenuation. Figure 7.21 shows biological absorption spectra that were previously inaccessible for study and analysis.

7.6 Superresolution Quantum Microscopy

7.6.1 Subwavelength Quantum Microscopy

The measurement of small distances is a fundamental problem of interest since the early days of science. It has become even more important due to recent interest in nanoscopic and mesoscopic phenomena in biophysics. Starting from the invention of the optical microscope around 400 years ago, today's optical microscopy methodologies can basically be divided into lens-based and lensless imaging. In general, far-field imaging is lens-based and thus limited by criteria such as the Rayleigh diffraction limit which states that the achievable resolution in the focus plane is limited to approximately half of the wavelength of illuminating light. Further limitation arises from out-of-focus light, which affects the resolution in the direction perpendicular to the focal plane.

Many methods have been suggested to break these limits. Lens-based techniques include confocal, nonlinear femtosecond, or stimulated emission depletion microscopy which have been recognized by the Nobel Prize. They have achieved remarkable first results, as shown in Fig. 7.1. Also non-classical features such as entanglement, quantum interferometry, or multi-photon processes can be used to enhance resolution. However, there is still great interest in achieving nanometer distance measurements by using optical illuminating far-field imaging only.

Recently, new schemes were proposed [45–47] to measure the distance between two adjacent two-level systems by driving them with a standing wave laser field and measuring the far-field resonance fluorescence spectrum, which is motivated by the localization of single atom inside a standing wave field to distances smaller than the Rayleigh limit $\lambda/2$. The basic idea is that in a standing wave, the effective driving field strength depends on the position of the particles (Fig. 7.22). Thus, each particle generates a sharp sideband peak in the spectrum, where the peak position directly relates to the subwavelength position of the particle. As long as the two sideband peaks can be distinguished from each other, the position of each particle can be recovered. However, when the interatomic distance decreases, the two particles can no longer be considered independent. Due to the increasing dipole–dipole interaction between the two particles, the fluorescence spectrum becomes complicated. It was found, however, that the

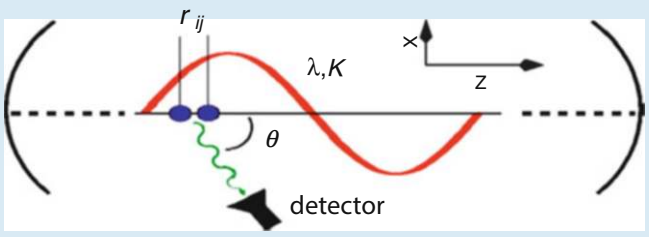

Fig. 7.22 Two atoms in a standing wave field separated by a distance r_{ij} smaller than half of the wavelength λ of the driving field. The distance of the two atoms is measured via the emitted resonance fluorescence

dipole–dipole interaction energy can directly be extracted from the fluorescence spectrum by adjusting the parameters of the driving field. Since the dipole–dipole interaction energy is distance dependent, it yields the desired distance information. The new schemes showed the applicability to inter-particle distances in a very wide range from $\lambda/2$ to about $\lambda/550$. These schemes can be extended for sensing the inter-molecular distances with applications in molecular and cellular biology, microbiology, and medical research leading to precision resolution in microorganisms such as protozoa, bacteria, molds, and sperms. Other applications would involve mapping of DNA.

7.6.2 Tip-Enhanced Quantum Bioimaging

Understanding the structure–function relationships of molecular constituents of biological pathogens is important for building more precise models and for the design of bacteria inactivating drugs, etc. Pathogenic diseases that are caused by viral pathogens include smallpox, influenza, mumps, measles, chickenpox, ebola, etc. New technology is needed for rapid detection and treatment, and for detailed studies of nanoscale components of pathogens with high spatial and temporal resolution and with simultaneous chemical analysis. Various nano-spectroscopic methods have been used to model pathogens. Direct imaging of the structural dynamics is challenging due to the small size of the biomolecules. Novel quantum optical techniques based on nanoscale sensors with high spatial and molecular-level resolution aim to improve the existing pathogen structure–property models.

Recent exceptional breakthroughs in the spatial resolution (<1 nm) make tip-enhanced Raman scattering (TERS), which is an important variation of SERS, a very powerful tool for in situ chemical analysis on the nanoscale. TERS has recently been applied to imaging biological systems. However, several challenges remain due to weak Raman signals and motion of live cells during long acquisition time imaging. We have performed such nanoantenna-tip-induced bio-sensing of bacteria and nanoscale imaging of biological cells (Fig. 7.23). The goal is to map the molecule–substrate interactions with nanoscale molecular-level spatial resolution in both topography (using atomic force microscopy (AFM)) and chemical identification (using Raman spectroscopy). Both electromagnetic and chemical enhancement effects can be used to identify the molecular biomarkers and nanoscale chemical surface properties of biological systems.

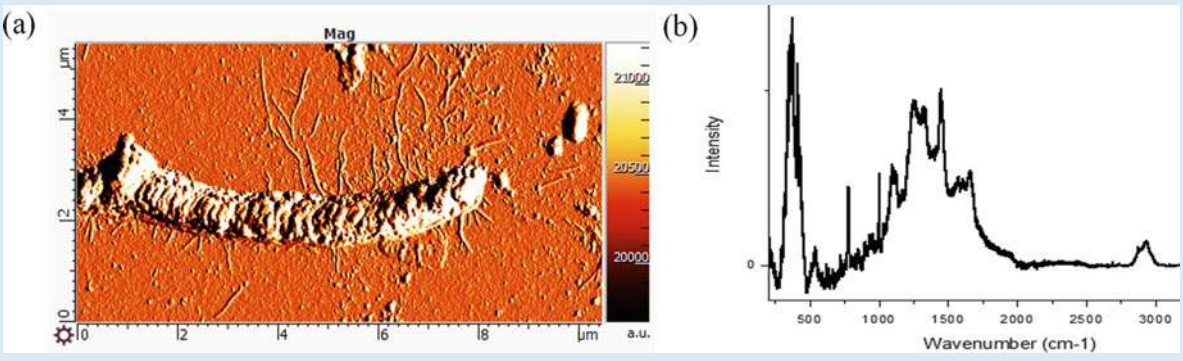

Fig. 7.23 (**a**) AFM image of a bacterial cell. (**b**) Typical Raman spectrum of bacteria

7.7 Novel Light Sources

7.7.1 Fiber Sensors

Recent research on fiber sensing has been focused on the development and demonstration of advanced fiber components and fiber-based strategies for quantum sensing. Fiber-bundle microprobe sensors have been developed using specifically designed fiber bundles and coupled to a confocal optical microscope to enable multiplex sensing, including multicolor in vivo detection of neuronal activity in a living brain using fluorescent protein biomarkers. Fiber-bundle microprobe sensors have also been used to confront the long-standing issues in practical imaging and sensing, including fiber-based endoscopic Raman imaging (Fig. 7.24).

Recent advances in optical magnetometry pave the ways toward an unprecedented spatial resolution and a remarkably high sensitivity in magnetic field detection, offering unique tools for the measurement of weak magnetic fields in a broad variety of areas from astrophysics, geosciences, and the physics of fundamental symmetries to medicine and life sciences. To unleash the full potential of this emerging technology and make it compatible with the requirements of practical quantum technologies and in vivo studies in life sciences, optical magnetometers have to be integrated with fiber-optic probes. This challenge has been addressed by developing a scanned fiber-optic probe for magnetic field imaging where nitrogen–vacancy (NV) centers are coupled to an optical fiber integrated with a two-wire microwave transmission line. The electron spin of NV centers in a diamond microcrystal attached to the tip of the fiber probe is manipulated by a frequency-modulated microwave field and is initialized by laser radiation transmitted through the optical tract of the fiber probe (Fig. 7.25) [50, 51]. The photoluminescence spin-readout return from NV centers is captured and delivered by the same optical fiber, allowing the two-dimensional profile of the magnetic field to be imaged with high speed and high sensitivity.

7.7.2 Quantum Coherence in X-Ray Laser Generation

The application of the techniques of quantum coherence and LWI to areas such as XUV and X-ray laser generation holds promise. The quantum coherence in atomic

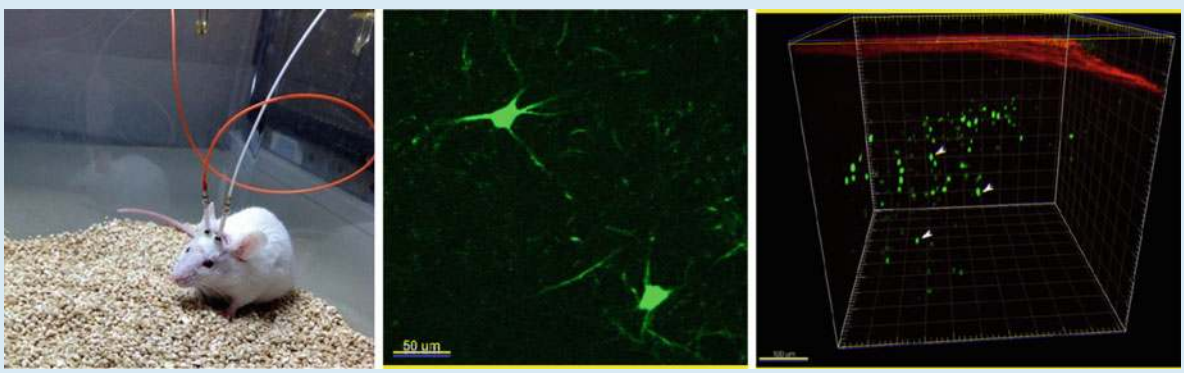

Fig. 7.24 Fiber-based sensing and imaging for neurophotonics and agricultural applications. Adapted from [48, 49]

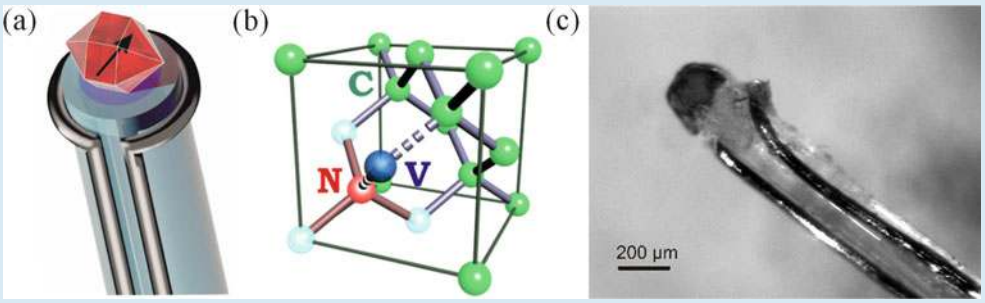

Fig. 7.25 (**a**) A fiber probe integrating an NV-diamond quantum sensor, an optical fiber, and a microwave transmission line. (**b**) A nitrogen atom (N) and a vacancy (V) forming an NV center in a diamond lattice, consisting of carbon (C) atoms. (**c**) Image of a prototype fiber-optic magnetometer and thermometer. Adapted from [50, 51]

and radiation physics has led to many interesting and unexpected consequences. For example, an atomic ensemble prepared in a coherent superposition of states yields self-induced transparency, photon echo, and coherent Raman beats [52, 53]. Another important coherence effect in atoms leads to phenomena of electromagnetically induced transparency, where by preparing an atomic system in a coherent superposition of states, under certain conditions, it is possible for atomic coherence to cancel absorption but not emission (Fig. 7.26). This is the basis for LWI, the essential idea being the absorption cancellation by atomic coherence and interference. Frequently this is accomplished in three- or four-level atomic systems in which there are coherent routes for absorption that can destructively interfere, thus leading to the cancellation of absorption. A small population in the excited state can thus lead to net gain, and this was the subject of substantial theoretical work by us several groups in the 1980s [24–26]. We have carried out the first LWI demonstrations in the mid-1990s [54, 55], and have recently continued in theoretical and experimental fronts to investigate the possibility of coherence driven lasing and lasing in XUV and soft X-ray regions [56, 57].

Existing X-ray laser sources such as X-ray free electron laser (X-FEL) at SLAC provided tremendous excitement for scientists in various disciplines. However, very large cost and size of this great device motivates researchers to search for portable, inexpensive XUV (see for example Suckewer, et al. [56]), and X-ray devices. On the other hand, the table top soft X-ray (SXL) and XUV lasers, due to their compactness, excellent beam quality, and very reliable operation in wavelength range of 10–50 nm hold great promise for tools for high resolution microscopy, micro-holography, very high plasma density measurements, semiconductor surface studies, and nano-lithography. Intensive efforts have been made to develop such compact soft X-ray lasers that are suitable for applications in academic and industrial laboratories as well as in the field biophotonics applications. LWI in the X-ray region would provide appealing opportunities and profound impacts on X-ray laser science as well as studies in the fields such as crystallography, solid materials, health sciences, high resolution microscopy of biological systems, and many more.

7.7.3 Coherent Control of Gamma Rays

Active control of light–matter interactions is an ultimate goal of many quantum biophotonics applications. Coherent control by laser pulse shaping has been a highly active research area for the last two decades addressing a large variety of problems including control of chemical reactions, spectroscopic signals, optical

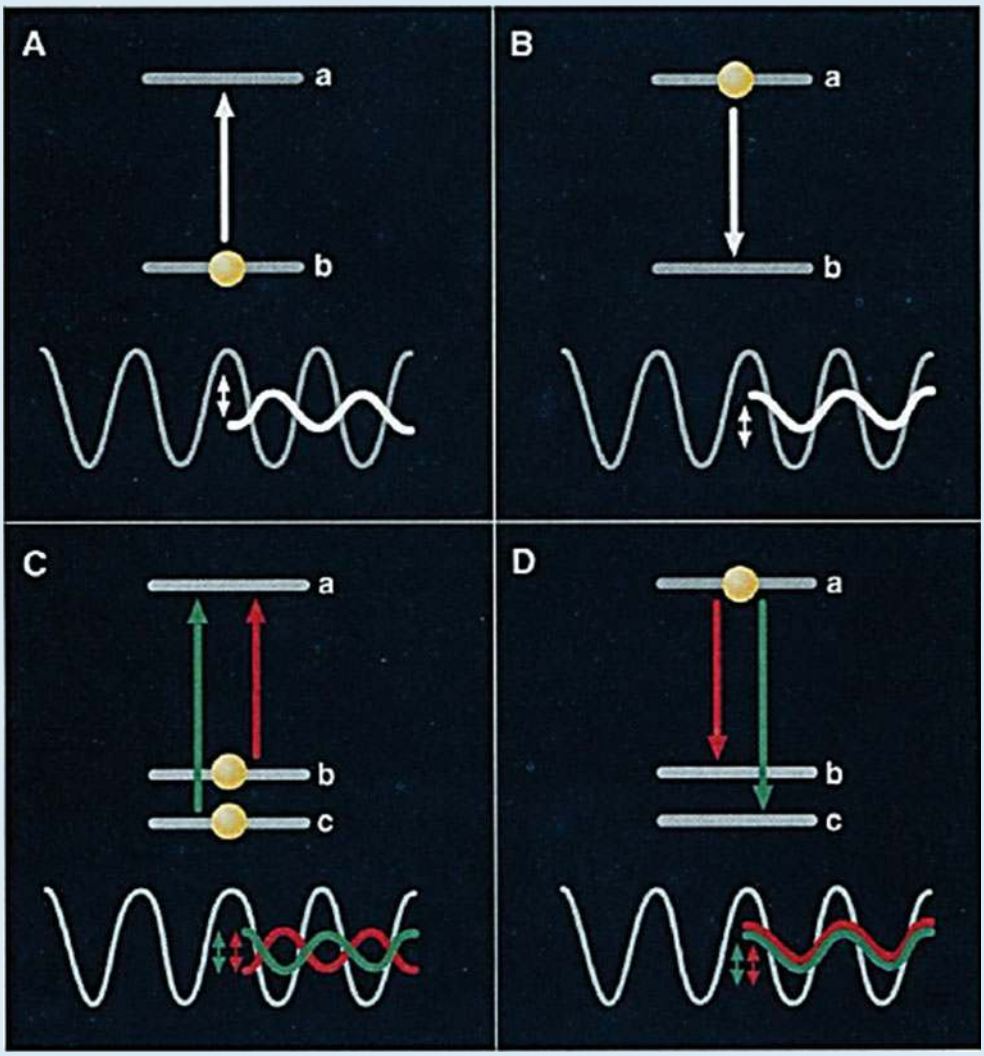

Fig. 7.26 Lasing without inversion (LWI) first experimentally realized at TAMU [54, 55]. Absorption cancellation by atomic coherence and interference is the basis for LWI. Adapted from [58]

sensors, microscopic images, photolithography, optical nanostructures, quantum logic operations, etc. All these applications, however, were aimed at controlling electronic motions, molecular vibrations and rotations using shaped electromagnetic radiation in the frequency range spanning from infrared to optical to ultraviolet range. The X-ray and gamma ray sources with controllable waveforms were up till now unavailable, and therefore there were no related applications.

Now, for the first time, we have an available source of controllable gamma rays [59]. Single ultrashort gamma ray pulses, double pulses, and pulse trains with controllable pulse delays can be produced (Fig. 7.27). Splitting of the single photon into two pulses constitutes the first realization of a time-bin qubit in this range of frequencies. The production of single-photon ultrashort-pulse trains with pulse duration much shorter than the natural lifetime of the emitting nuclear level and with the controllable waveforms provides a unique opportunity for the realization of quantum memories and other nuclear-ensemble—gamma-photons interfaces, opening the prospects for fascinating applications in quantum communication and information.

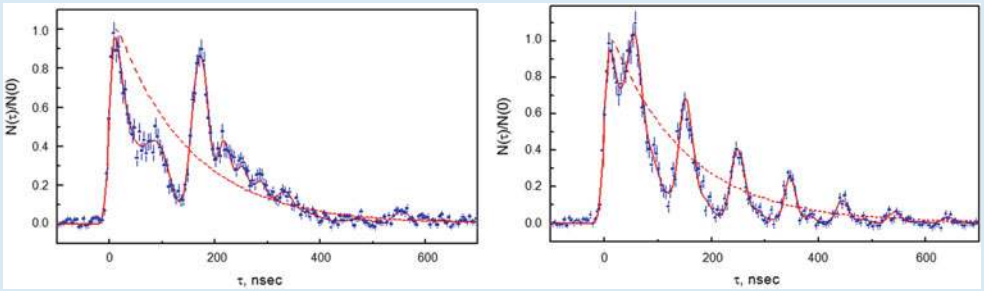

Fig. 7.27 Splitting gamma ray photons into double pulses (*left*) and multiple pulse trains (*right*). Adapted from [59]

The energy of these gamma ray pulses corresponds to nuclear transitions. This may enable, for the first time, coherent control of nuclear reactions. The parameters of the pulses can be widely controlled including the shape and number of pulses, repetition rate (potentially variable in the range from MHz to GHz), and duration (potentially ranged from 100 ns to 100 ps). This allows for a variety of time-resolved experiments (including dynamic X-ray diffraction). Gamma rays can provide an extremely high (potentially sub-Angstrom and currently nanometer) spatial resolution. The simultaneous high spatial and temporal resolution makes this technology promising for nanoscale ultrafast imaging of electronic motions in biomolecules and protein folding dynamics.

7.8 Conclusion

In summary, we have (hopefully) shown that at the interface between quantum optics and biophysics lies the emerging exciting field of quantum biophotonics. With new light sources and quantum techniques, it becomes increasingly possible to apply the techniques of quantum optics to biosciences. This will have major payoff in agriculture, environmental science, and national security, and promises to be the dawn of a new era in biophotonics emphasizing quantum effects.

Acknowledgment We acknowledge the support of the National Science Foundation Grants No. EEC-0540832 (MIRTHE ERC), No.PHY-1068554, No. PHY-1241032 (INSPIRE CREATIV), No. DBI-1455671, No. DBI-1532188, No. ECCS-1509268 and No. PHY-1307153, the Office of Naval Research grant N00014-16-1-3054, the US DOD awards FA9550-15-1-0517 and N00014-16-1-2578, and CPRIT grant RP160834, and the Robert A. Welch Foundation (Awards A-1261 and A-1547).

References

1. Wildanger D, Rittweger E, Kastrup L, Hell SW (2008) STED microscopy with a supercontinuum laser source. Opt Express 16:9614
2. Chmyrov A, Keller J, Grotjohann T, Ratz M, d'Este E, Jakobs S, Eggeling C, Hell SW (2013) Nanoscopy with more than 100,000 'doughnuts'. Nat Methods 10:737
3. Scully MO, Kattawar GW, Lucht RP, Opatrny T, Pilloff H, Rebane A, Sokolov AV, Zubairy MS (2002) FAST CARS: Engineering a laser spectroscopic technique for rapid identification of bacterial spores. Proc Natl Acad Sci U S A 99:10994
4. Pestov D, Murawski RK, Ariunbold GO, Wang X, Zhi M, Sokolov AV, Sautenkov VA, Rostovtsev YV, Dogariu A, Huang Y, Scully MO (2007) Optimizing the laser-pulse configuration for coherent Raman spectroscopy. Science 316:265
5. Pestov D, Wang X, Ariunbold GO, Murawski RK, Sautenkov VA, Dogariu A, Sokolov AV, Scully MO (2008) Single-shot detection of bacterial endospores via coherent Raman spectroscopy. Proc Natl Acad Sci U S A 105:422
6. Arora R, Petrov GI, Yakovlev VV, Scully MO (2012) Detecting anthrax in the mail by coherent Raman microspectroscopy. Proc Natl Acad Sci U S A 109:1151
7. Bixler LN, Cone MT, Hokr BH, Mason JD, Figueroa E, Fry ES, Yakovlev VV, Scully MO (2014) Ultrasensitive detection of waste products in water using fluorescence emission cavity-enhanced spectroscopy. Proc Natl Acad Sci U S A 111:7208
8. Voronine DV, Sinyukov AM, Xia H, Wang K, Jha PK, Welch G, Sokolov AV, Scully MO (2012) Time-resolved surface-enhanced coherent sensing of nanoscale molecular complexes. Sci Rep 2:891
9. Lis D, Cecchet F (2014) Localized surface plasmon resonances in nanostructures to enhance nonlinear vibrational spectroscopies: towards an astonishing molecular sensitivity. Beilstein J Nanotechnol 28:2275
10. Altangerel N, Ariunbold G, Gorman C, Bohlmeyer D, Yuan J, Hemmer P, Scully MO (2016) Early, in vivo, detection of abiotic plant stress responses via Raman spectroscopy. Conference on Lasers and Electro-Optics OSA Technical Digest (Optical Society of America, 2016), paper SF1H.3. doi:► 10.1364/CLEO_SI.2016.SF1H.3
11. Palombo F, Madami M, Stone N, Fioretto D (2014) Mechanical mapping with chemical specificity by confocal Brillouin and Raman microscopy. Analyst 139:729
12. Traverso AJ, Thompson JV, Steelman ZA, Meng Z, Scully MO, Yakovlev VV (2015) Dual Raman-Brillouin microscope for chemical and mechanical characterization and imaging. Anal Chem 87:7519
13. Meng Z, Traverso AJ, Yakovlev VV (2014) Background clean-up in Brillouin microspectroscopy of scattering medium. Opt Express 22:5410
14. Petrov GI, Arora R, Yakovlev VV, Wang X, Sokolov AV, Scully MO (2007) Comparison of coherent and spontaneous Raman microspectroscopies for noninvasive detection of single bacterial endospores. Proc Natl Acad Sci U S A 104:7776
15. Hemmer PR, Miles RB, Polynkin P, Siebert T, Sokolov AV, Sprangle P, Scully MO (2011) Standoff spectroscopy via remote generation of a backward-propagating laser beam. Proc Natl Acad Sci U S A 108:3130
16. Dogariu A, Michael JB, Scully MO, Miles RB (2011) High-gain backward lasing in air. Science 331:442
17. Traverso AJ, Sanchez-Gonzalez R, Yuan L, Wang K, Voronine DV, Zheltikov AM, Rostovtsev Y, Sautenkov VA, Sokolov AV, North SW, Scully MO (2012) Coherence brightened laser source for atmospheric remote sensing. Proc Natl Acad Sci U S A 109:15185
18. Kocharovsky V, Cameron S, Lehmann K, Lucht R, Miles R, Rostovtsev Y, Warren W, Welch GR, Scully MO (2005) Gain-swept superradiance applied to the stand-off detection of trace impurities in the atmosphere. Proc Natl Acad Sci U S A 102:7806
19. Cremers DA, Radziemski LJ (2006) Handbook of laser-induced breakdown spectroscopy 302. John Wiley, West Sussex
20. Mitrofanov AV, Voronin AA, Sidorov-Biryukov DA, Pugžlys A, Stepanov EA, Andriukaitis G, Flöry T, Ališauskas T, Fedotov AB, Baltuška A, Zheltikov AM (2014) Mid-infrared laser filaments in the atmosphere. Sci Rep 5:8368

21. Malevich PN, Kartashov D, Ališauskas ZPS, Pugžlys A, Baltuška A, Giniūnas L, Danielius R, Lanin AA, Zheltikov AM, Marangoni M, Cerullo G (2012) Ultrafast-laser-induced backward stimulated Raman scattering for tracing atmospheric gases. Opt Express 20:18784
22. Malevich PN, Maurer R, Kartashov D, Ališauskas S, Lanin AA, Zheltikov AM, Marangoni M, Cerullo G, Baltuška A, Pugžlys A (2015) Stimulated Raman gas sensing by backward UV lasing from a femtosecond filament. Opt Lett 40:2469
23. Kocharovskaya O, Khanin YI (1988) Coherent amplification of an ultrashort pulse in a three-level medium without a population inversion. JETP Lett 48:630
24. Harris SE (1989) Lasers without inversion: interference of lifetime-broadened resonances. Phys Rev Lett 62:1033
25. Scully MO (1985) Correlated spontaneous-emission lasers: quenching of quantum fluctuations in the relative phase angle. Phys Rev Lett 55:2802
26. Scully MO, Zhu SY, Gavrielides A (1989) Degenerate quantum-beat laser: lasing without inversion and inversion without lasing. Phys Rev Lett 62:2813
27. Scully MO (2010) Quantum photocell: using quantum coherence to reduce radiative recombination and increase efficiency. Phys Rev Lett 104:207701
28. Scully MO, Chapin KR, Dorfman KE, Kim M, Svidzinsky AA (2011) Quantum heat engine power can be increased by noise-induced coherence. PNAS 108:15097
29. Dorfman KE, Voronine DV, Mukamel S, Scully MO (2013) Photosynthetic reaction center as a quantum heat engine. PNAS 110:2746
30. Scully MO, Zubairy MS, Agarwal GS, Walther H (2003) Extracting work from a single heat bath via vanishing quantum coherence. Science 299:862
31. Sarovar M, Ishizaki A, Fleming GR, Whaley KB (2010) Quantum entanglement in photosynthetic light-harvesting complexes. Nat Phys 6:462
32. Engel GS, Calhoun TR, Read EL, Ahn TK, Mancal T, Cheng YC, Blankenship RE, Fleming GR (2007) Evidence for wavelike energy transfer through quantum coherence in photosynthetic systems. Nature 446:782
33. Collini E, Wong CY, Wilk KE, Curmi PM, Brumer P, Scholes GD (2010) Coherently wired light-harvesting in photosynthetic marine algae at ambient temperature. Nature 463:644
34. Panitchayangkoon G, Hayes D, Fransted KA, Caram JR, Harel E, Wen J, Blankenship RE, Engel GS (2010) Long-lived quantum coherence in photosynthetic complexes at physiological temperature. Proc Natl Acad Sci U S A 107:12766
35. Brixner T, Stenger J, Vaswani HM, Cho M, Blankenship RE, Fleming GR (2005) Two-dimensional spectroscopy of electronic couplings in photosynthesis. Nature 434:625
36. Abramavicius D, Palmieri B, Voronine DV, Sanda F, Mukamel S (2009) Coherent multidimensional optical spectroscopy of excitons in molecular aggregates; quasiparticle versus supermolecule perspectives. Chem Rev 109:2350
37. Kozlov VV, Rostovtsev Y, Scully MO (2006) Inducing quantum coherence via decays and incoherent pumping with application to population trapping, lasing without inversion, and quenching of spontaneous emission. Phys Rev A 74:063829
38. Panitchayangkoon G, Voronine DV, Abramavicius D, Mukamel D, Engel GS (2011) Direct evidence of quantum transport in photosynthetic light harvesting complexes. PNAS 108:20908
39. Yanik AA, Huang M, Kamohara O, Artar A, Geisbert TW, Connor JH, Altug H (2010) An optofluidic nanoplasmonic biosensor for direct detection of live viruses from biological media. Nano Lett 10:4962
40. Fry ES, Kattawar GW, Pope RM (1992) Integrating cavity absorption meter. Appl Opt 31:2055
41. Pope RM, Fry ES (1997) Absorption spectrum (380-700 nm) of pure water: II. Integrating cavity measurements. Appl Opt 36:8710
42. Labsphere (2006) A guide to reflectance coatings and materials. Tech. Rep. ► http://www.labsphere.com
43. Cone MT, Musser JA, Figueroa E, Mason JD, Fry ES (2015) Diffuse reflecting material for integrating cavity spectroscopy—including ring-down spectroscopy. Appl Opt 54:334
44. Cone MT, Mason JD, Figueroa E, Hokr BH, Bixler JN, Castellanos CC, Wigle JC, Noojin GD, Rockwell BA, Yakovlev VV, Fry ES (2015) Measuring the absorption coefficient of biological materials using integrating cavity ring-down spectroscopy. Optica 2:162
45. Chang JT, Evers J, Scully MO, Zubairy MS (2006) Measurement of the separation between atoms beyond diffraction limit. Phys Rev A 73:031803
46. Chang JT, Evers J, Zubairy MS (2006) Distilling two-atom distance information from intensity-intensity correlation functions. Phys Rev A 74:043820
47. Liao Z, Alamri M, Zubairy MS (2012) Resonance-fluorescence-localization microscopy with subwavelength resolution. Phys Rev A 85:023810

48. Doronina-Amitonova LV, Fedotov IV, Ivashkina OI, Zots MA, Fedotov AB, Anokhin KV, Zheltikov AM (2013) Implantable fiber-optic interface for parallel multisite long-term optical dynamic brain interrogation in freely moving mice. Sci Rep 3:3265
49. Doronina-Amitonova LV, Fedotov IV, Fedotov AB, Anokhin KV, Zheltikov AM (2015) Neurophotonics: optical methods to study and control the brain. Phys Usp 58:345
50. Fedotov IV, Safronov NA, Shandarov YA, Lanin AA, Fedotov AB, Kilin SY, Sakoda K, Scully MO, Zheltikov AM (2012) Guided-wave-coupled nitrogen vacancies in nanodiamond-doped photonic-crystal fibers. Appl Phys Lett 101:031106
51. Fedotov IV, Doronina-Amitonova LV, Voronin AA, Levchenko AO, Zibrov SA, Sidorov-Biryukov AD, Fedotov AB, Velichansky VL, Zheltikov AM (2014) Electron spin manipulation and readout through an optical fiber. Sci Rep 4:5362
52. Zhu SY, Nikonov DE, Scully MO (1998) A scheme for noninversion lasing for short-wavelength lasers in helium like ions. Found Phys 28:611
53. Rostovtsev Y, Scully MO (2007) Soft X-ray lasing without population inversion in ^{3}He using Pauli principle. J Mod Opt 54:2607
54. Zibrov AS, Lukin MD, Nikonov DE, Hollberg L, Scully MO, Velichansky VL, Robinson HG (1995) Experimental demonstration of laser oscillation without population inversion via quantum interference in Rb. Phys Rev Lett 75:1499
55. Padmabandu GG, Welch GR, Shubin IN, Fry ES, Nikonov DE, Lukin MD, Scully MO (1996) Laser oscillation without population inversion in a sodium atomic beam. Phys Rev Lett 76:2053
56. Sete EA, Svidzinsky AA, Rostovtsev YV, Eleuch H, Jha PK, Suckewer S, Scully MO (2011) Using quantum coherence to generate gain in the XUV and X-ray: Gain-swept superradiance and lasing without inversion. IEEE J Sel Top Quantum Electron 18:541
57. Xia H, Svidzinsky AA, Yuan L, Lu S, Suckewer S, Scully MO (2012) Observing superradiant decay of excited-state helium atoms inside helium plasma. Phys Rev Lett 109:093604
58. Scully MO, Fleischhauer M (1994) Lasers without inversion. Science 263:337
59. Vagizov F, Antonov V, Radeonychev YV, Shakhmuratov RN, Kocharovskaya O (2014) Coherent Control of the waveforms of recoilless gamma-photons. Nature 508:80